A RING COLLECTION SPECTROMETER

INVESTIGATION OF THE DECAY OF Sb 125

by

FRANK ALDEN PAYNE

B.A.Sc. The University of British Columbia, 1954
M.A.Sc. The University of British Columbia, 1957

A THESIS SUBMITTED IN PARTIAL FULFILMENT OF

THE REQUIREMENTS FOR THE DEGREE OF

DOCTOR OF PHILOSOPHY

in the Department

of

PHYSICS

We accept this thesis as conforming to

the required standard

THE UNIVERSITY OF BRITISH COLUMBIA

April, 1961

In presenting this thesis in partial fulfilment of the requirements for an advanced degree at the University of British Columbia, I agree that the Library shall make it freely available for reference and study. I further agree that permission for extensive copying of this thesis for scholarly purposes may be granted by the Head of my Department or by his representatives. It is understood that copying or publication of this thesis for financial gain shall not be allowed without my written permission.

Department of PHYSICS

The University of British Columbia,
Vancouver 8, Canada.

Date April 6, 1961.

ABSTRACT

A thin-lens beta-ray spectrometer has been modified for collection of beta-rays at the position of the ring focus. This has increased the gathering power/line width ratio from $\backsim$ 0.12 to $\backsim$ 0.8. The focusing properties of the instrument have been investigated for various geometries.

Using the modified spectrometer, the decay scheme of Sb 125 - Te 125 has been investigated. The primary beta spectrum, photoelectron spectra and beta-gamma coincidence spectra have been measured.

From conversion coefficient measurements, the following radiative transition multipolarities were determined (energies in kev): 176(E2+M1), 428(E2+M1), 464(E2), 602(E2+M1) and 638(E2).

Five primary beta groups have been identified with end point energies of 626, 450, 307, 246 and 133 kev. Previously unobserved transitions of 76, 143, 219, 355, 540 and 640 kev have been identified.

Based on all experimental evidence the following states of Te 125 with spin and parity assignments have been proposed: ground state ($s_{1/2+}$), 36 kev ($d_{3/2+}$), 145 kev ($h_{11/2^-}$), 321 kev (9/2-), 464 kev (5/2+), 525 kev (11/2- or 9/2-), 540 kev (11/2- or 9/2-), 638 kev (5/2+) and 676 kev (spin and parity undetermined).

TABLE OF CONTENTS

LIST OF FIGURES AND TABLES

CHAPTER III

ACKNOWLEDGEMENTS

The work involved in this thesis has been facilitated by the advice and assistance of many people.

I would like to thank Mr. Alex Fraser and Mr. William Morrison for their technical advice and for the construction of parts of the apparatus.

Thanks are also due to Mr. H. R. Schneider for the use of his coincidence apparatus, Mr. H. R. Schneider and Mr. E. D. Earle for their investigation of the sensitivities of several photomultipliers and to Dr. J. B. Warren for the use of the kicksorter.

Most of all, to Dr. K. C. Mann, who suggested the research problem, I wish to express my sincere appreciation for his assistance throughout the experimental investigation and the analysis of the results.

Finally I wish to thank the National Research Council for awarding me Studentships during the period 1957-1959 and the Defense Research Board for financial support from 1959 until the completion of this thesis.

CHAPTER I

NUCLEAR DECAY AND NUCLEAR SPECTROSCOPY

I. Introduction

Nuclear physics may be defined generally to be the study of the physical properties of the nucleus - its physical structure, electrical and mechanical properties, and modes of excitation. The main structural or mechanical properties of the nucleus are mass, size, shape and angular momentum while typical electric and magnetic properties associated with the nucleus are charge, magnetic dipole moment and electric quadrupole moment. There are, of course, many ways whereby nuclear properties may be investigated. One very powerful method is the investigation and classification of the radiations emitted by a radioactive nucleus. This is the field of nuclear spectroscopy.

It is observed that a nucleus can exist in various discrete states with each of which is associated a total energy for the nucleus. The state having the lowest associated energy is called the ground state of the nucleus while

states of higher energy are called excited states. If a nucleus is in an excited state, it is in an unstable configuration and it decays to a state of lower energy, usually giving up the excess energy by the emission of electromagnetic radiation (gamma-rays). In this case it eventually reaches its ground state which may or may not be stable against further decay. If the ground state configuration of the nucleus is a stable one, the nucleus is then a nucleus of a stable isotope of one of the elements in the periodic table. If the ground state configuration is not stable, the nucleus then decays by one of several possible processes with a possible resulting change in nuclear charge. This means that the original nucleus becomes a different nucleus, its atom a different atom in terms of chemical behaviour, and is classified as an isotope of a different element in the periodic table.

The three most common processes by which the unstable ground state of a nucleus can decay are by the emission of a negatron or positron or by orbital electron capture, all processes being called beta decay and in each case resulting in a change of nuclear charge. The occurrence of these types of decay is possible if:

$$\left.\begin{array}{ll} M(Z,A) > M(Z+1,A) & \text{for negatron emission} \\ M(Z,A) > M(Z-1,A) + 2m_o & \text{for positron emission} \\ M(Z,A) > M(Z-1,A) & \text{for orbital electron capture} \end{array}\right\} \quad (1)$$

where m is the mass of the electron and M(Z,A) is the atomic mass of the neutral atom having Z protons and mass number A.

II. Beta Decay

a) Theory

Beta-rays are experimentally indistinguishable from atomic electrons. They display the same e/m value and the same charge and are observed not to be captured by atomic orbits already occupied by electrons. Thus they are excluded from filled electron states by the Pauli principle and hence they are identical particles.

Beta spectra are unique among nuclear spectra in that they are observed to be continuous in energy, approaching zero intensity at small energies, passing through a maximum and returning to zero intensity again at some end point energy, E_o, which has been shown to be the available decay energy. This fact appears to violate the law of conservation of energy except at the one energy E_o. Also, it is observed that beta decay occurs between nuclear states whose angular momentum, measured in units of $\hbar$, differs by integral values. This is not compatible with the half-integral spin associated with the electron and with the law of conservation of angular momentum. These discrepancies are overcome by the neutrino

hypothesis of Pauli, in which is postulated the simultaneous emission of the neutrino and beta particle. To preserve the conservation laws of angular momentum and energy, the neutrino is assumed to have an intrinsic spin of $\hbar/2$, an energy of $(E_o - E_\beta)$ and a very small or zero mass.

The quantum mechanical theory of beta decay was first formalized by Fermi[1] in 1934. In its simpler form he made the following assumptions:

(a) The wave functions of the neutrino and electron may be approximated by plane waves.

(b) The probability of beta decay depends upon the expectation value of finding the electron and the neutrino at the nucleus.

(c) The probability of emission depends upon unknown factors such as the matrix element M taken between the initial and final states of the nucleus and a constant factor, g, representing the strength of the coupling giving rise to the interaction.

In mathematical language these assumptions take the form:

(a) If ψ_β, $\bar{p}_\beta$ and ψ_ν, $\bar{p}_\nu$ are the wave functions and momenta representing the beta particle and neutrino respectively, then:

$$\psi_\beta = N_\beta \, e^{i\bar{p}_\beta \cdot \frac{\bar{r}}{\hbar}} \; ; \quad \psi_\nu = N_\nu \, e^{i\bar{p}_\nu \cdot \frac{\bar{r}}{\hbar}} \tag{2}$$

are the plane wave forms of the wave functions in which N_β and N_ν are normalization factors.

(b) The expectation value for finding the beta particle and the neutrino at the nucleus is given by:

$$|\psi_\beta(0)|^2 \cdot |\psi_\nu(0)|^2 \qquad (3)$$

(c) The uncertainty with regard to the nature of the interaction causing the decay permits M to be of several possible forms. Two such forms are:

$$M = \int \psi_f^* \psi_i \, d\tau \qquad (4a)$$

$$M = \int \psi_f^* \bar{\sigma} \psi_i \, d\tau \qquad (4b)$$

for the scalar and tensor interactions respectively, where ψ_f and ψ_i are the wave functions describing the final and initial states of the nucleus and $\bar{\sigma}$ is a generalization of the Pauli spin matrices. Three other types of interactions are also possible, namely the pseudoscalar, polar vector and axial vector interactions. It remains for experimental evidence to determine which form of the matrix element and therefore which type of interaction best describes the results observed.

The momentum distribution of emitted beta particles based on the above assumptions turns out to be:

$$p(p)dp = C \, |M|^2 \, (E_o - E)^2 \, p^2 dp \qquad (5)$$

where E is the total electron energy in units of $m_o c^2$

p is the electron momentum in units $m_o c$

$C = g^2/2\pi^3\hbar^7 c^3$.

As previously noted, a plane wave solution for the electron wave function has been assumed. This assumption is, in fact, too crude and if the distortion to the electron wave function by the nuclear coulomb field is taken into account by a factor F(Z,p) then equation (5) becomes:

$$P(p)dp = C|M|^2 F(Z,p) (E_o-E)^2 p^2 dp \qquad (6)$$

The coulomb effect on the wave function of an emitted electron is, of course, different from the coulomb effect for positron emission because of the difference in sign of the charge of the two particles. This effect is most marked at low energies where the negatron momentum distribution is increased and the positron momentum distribution is decreased because of the respective attraction and repulsion of the negatron and positron.

In the calculation of M in the above treatment, each of the wave functions is expressed as a series in powers of $(R/\lambda\!\!\!^{-})$ where R is the radial extension of the nucleus and $\lambda\!\!\!^{-}$ corresponds to the wavelength of the emitted beta particle. If one assumes zero extension of the nucleus as in the above treatment, or in other words if one considers only the first

term in the series expansion of the wave functions, then the momentum distribution resulting is that of a so-called "allowed" beta transition for which M is constant. When higher order terms are taken into account, the matrix element becomes a function of momentum and thus M is no longer a constant. The momentum distributions resulting from considering these higher order terms are those of the so-called "forbidden" transitions in which first-forbidden, second-forbidden and so on refer to the inclusion of the second, third and higher order terms respectively in the series expansion of the wave functions.

b) Selection Rules

For both allowed and forbidden spectra, certain selection rules govern the change of the two quantum characteristics, total angular momentum and parity. The angular momentum of a state when expressed in units of $\hbar$ gives the spin, I, of the state. Parity describes the nature of the wave function under inversion of its spacial coordinates and is said to be odd if the wave function changes sign under spacial inversion and even if it does not change sign under spacial inversion.

The selection rules which apply to a particular beta transition are dependent upon the nature of the matrix element used to describe the transition. For example, the

use of the matrix element in equation (4a) leads to the Fermi selection rules which for an allowed spectrum are:

$$\text{Fermi:} \qquad \Delta I = 0 \;\; ; \;\; \text{"no"}$$

This is a short hand notation meaning that the transition takes place between nuclear states of the same spin and parity. Hence $\Delta I = 0$ and there is "no" change in parity. Similarly, if the matrix element has the tensor form, as in equation (4b), the resulting selection rules, or Gamow-Teller selection rules, for an allowed transition are:

$$\text{G - T:} \quad \Delta I = 0, \pm 1 \;\; ; \;\; \text{"no"} \;\; ; \;\; \text{no } 0 \rightarrow 0.$$

Forbidden spectra have associated with them different selection rules governing spin change and parity change. Experimental evidence favours the G-T selection rules and therefore supports the tensor form of the interaction over the scalar form.

It should be noted here that the above treatment is a non-relativistic formulation and is therefore an oversimplification. A complete relativistic treatment gives rise to different selection rules for the various types of interactions and serves to explain a great many of the observed transitions. However, some transitions have been observed which cannot be explained by either the Fermi or Gamow-Teller selection rules. The problem of fitting these

transitions into the theory is as yet unresolved. In addition, the simple selection rules above cannot hope to explain the nature of forbidden spectra which may arise from complex relativistic interactions. One exception to this, however, is predicted by the theory in the case of transitions satisfying the conditions $\Delta I = n+1$; $\pi_i \pi_f = (-1)^n$, where n is the degree of forbiddenness. These transitions have a unique energy dependence for each n and are called "n^{th}-forbidden unique transitions".

c) Comparative Lifetime

The lifetime, t, of a beta transition is determined by integrating equation (6) to get:

$$\frac{1}{t} = C \quad f(Z,p_{max}) \quad |M|^2 \tag{7}$$

where

$$f(Z,p_{max}) = \int_o^{p_{max}} F(Z,p) \ (E_o-E)^2 \ p^2 dp$$

The function $f(Z,p_{max})$ has been extensively calculated and tabulated.[2] Thus the product ft, known as the comparative lifetime, is expressible as:

$$ft = \frac{\text{constant}}{|M|^2} \tag{8}$$

From this equation it can be seen that the comparative lifetime is a measure of the magnitude of the matrix element

associated with the transition. In general terms, the matrix element decreases with increasing order of forbiddenness thus making the ft-value a useful quantity in determining whether a transition is allowed or forbidden. In practise the quantity $\log_{10}$ft is used because the ft values vary over such a large range of magnitudes. Convenient methods of calculating log ft have been described by Moskowski.[3]

d) Kurie Plot

From equation (6) it can be seen that the beta spectrum approaches the end point energy E_o tangentially making E_o difficult to determine. This problem is overcome with the use of a Kurie plot which is simply a plot of

$\sqrt{\frac{N(p)}{p^2F}}$ versus E, where N(p) is the number of beta particles counted per unit momentum interval and is, of course, directly proportional to P(p). For this purpose F(Z,p) has been extensively calculated and tabulated.[4] For the allowed spectrum shape, in which M is constant, the Kurie plot results in a straight line with energy intercept E_o. The advantage of the Kurie plot lies in the fact that more weight may be placed on points having greater statistical accuracy than those near the end point.

In the case of a forbidden transition, the Kurie plot may not be linear and a shape correction factor[5] is introduced to make it linear. The degree of forbiddenness of

the transition can sometimes be determined by knowing which shape factor will linearize the Kurie plot. That is, the shape factor indirectly is a correction for the momentum dependence of the matrix element M and therefore can indicate whether a transition is allowed or forbidden. This is, however, not always a positive indication of whether a transition is allowed or forbidden because there are many cases of forbidden transitions having momentum independent matrix elements and whose Kurie plots are therefore linear.

e) Orbital Electron Capture

The process of orbital electron capture takes place entirely within the atom and is therefore difficult to observe. It manifests itself only through soft x-ray emission or Auger electron emission arising from the subsequent filling of the hole in the atomic shell structure caused by the electron capture. Since the orbital electron is captured from a bound state, the neutrino emitted by the nucleus has a discrete energy. Thus, in contrast to negatron and positron emission, the final states available in phase space are determined solely by the energy of the emitted neutrino. Another difference arises in the calculation of the probability for finding an orbital electron at the nucleus. In the theory of beta decay, the quantization was formulated within a box of volume V, and the probability of finding an electron

at the nucleus therefore depended upon the magnitude of V. The probability of finding an orbital electron at the nucleus, on the other hand, is independent of V and depends only on the shape of its orbit. Thus the atomic electron wave functions are used in this case.

It should be noted that most transitions of this type involve the capture of an electron from the atomic K-shell because the K-shell wave function overlaps the nuclear volume more than the wave functions of other shells. L-shell capture is of course possible but much less probable. Under the conditions that the energy in a transition is less than the binding energy of the K-shell electrons, then L-shell capture is predominant, but this condition is rarely met.

Whereas the density of final states for negatron and positron emission is of the form:

$$\rho(E_o) = \frac{V^2}{4\pi^4\hbar^6c^3}(E_o-E)^2\,p^2dp \qquad (9)$$

the corresponding expression for K-capture is:

$$\rho(E_\nu) = \frac{V}{2\pi^2\hbar^3c^3}(E_o+mc^2-E_B)^2 \qquad (10)$$

where E_B is the atomic binding energy of the captured electron.

As in negatron and positron emission, it is possible to write an expression for the lifetime of a K-capture

transition in the form:

$$\frac{1}{t_k} = \text{constant} \cdot f_k \tag{11}$$

where

$$f_k = 2\pi \left(\frac{Ze^2}{\hbar c}\right)^3 \left[E_o + 1 - \frac{1}{2}\left(\frac{Ze^2}{\hbar c}\right)^2\right]^2 \tag{12}$$

It should be emphasized that Z in equation (12) refers to the parent nucleus and not the daughter nucleus as in negatron and positron emission.

III. Gamma Decay

In general, radioactive decay by either beta emission or electron capture leaves the daughter nucleus in an excited state. This state then decays by either electromagnetic radiation or by the competing process of internal conversion, to be discussed later.

The quantum theory of radiation classifies gamma rays into electric and magnetic multipole radiations characterized, just as in particle emission, by the quantum mechanical properties of angular momentum, L, and parity, π, of the emitted photon. In classical analogy, these radiations arise from the oscillation of electric and magnetic nuclear multipoles which in turn are the result of the distribution of electric charge and currents in the nucleus. When a

nucleus decays from one excited state of spin I_i and parity π_i to another state of spin I_f and parity π_f, a gamma ray is emitted carrying away with it angular momentum $\bar{L} = |\bar{I}_i - \bar{I}_f|$ and parity $\pi_i \pi_f$, where $\pi = +1$ and -1 denotes even and odd parity respectively.

The multipolarity of a transition is defined to be 2^L for both magnetic and electric transitions. The probability for a transition between states having wave functions ψ_i and ψ_f is proportional to $\int \psi_f^* \, q \, \psi_i \, d\tau$, where $d\tau$ is a volume element and the operator q depends upon the type of transition. In the case of electric dipole radiation (El) for example, q will have the form $\sum e_i x_i$, which is an odd function. Thus El radiation has odd parity ($\pi = -1$) and in general E(L) radiation has parity $\pi = (-1)^L$. Similarly, M(L) radiation has parity $\pi = -(-1)^L$ in accord with the even or odd nature of q in $\int \psi_f^* \, q \, \psi_i \, d\tau$.

Conservation of angular momentum demands that $\bar{L} = |\bar{I}_i - \bar{I}_f|$ and it follows therefore that:

$$|I_i - I_f| \leq L \leq |\bar{I}_i + \bar{I}_f| \qquad (13)$$

In the theory of multipole radiation, transition probability decreases sharply with increasing multipolarity. Thus for most cases $L = |I_i - I_f| = \Delta I$. This, coupled with the fact that the probability of electric multipole radiation is generally much greater than the probability of magnetic

multipole radiation would lead one to expect that a transition involving a spin change ΔI would be a $2^{\Delta I}$-pole electric transition. Parity considerations, however, can sometimes make a $2^{\Delta I}$-pole magnetic multipole transition more probable.

The selection rules for gamma radiation during the transition $\psi_i \rightarrow \psi_f$ may be summarized as:

E(L) radiations - $\Delta I = L$; $\pi_i \pi_f = (-1)^L$

M(L) radiations - $\Delta I = L$; $\pi_i \pi_f = -(-1)^L$

No $0 \rightarrow 0$ transitions

The parity and L dependence of electric and magnetic multipole radiations allow the possibility of mixed transitions in which M(L) and E(L+1) are competing multipoles. So far, only E2+M1 mixtures have been experimentally observed.

IV. Internal Conversion

Whenever a nucleus decays by multipole radiation, the competing process of internal conversion is also possible. In this process, the excitation energy of the transition is given up to one of the bound atomic electrons. The electron is emitted with an energy:

$$E = E_o - E_B \qquad (14)$$

where E_o is the energy of the transition

E_B is the binding energy of the electron in

its atomic orbit.

Internal conversion may take place through interaction with an electron in any of the atomic levels but K-shell conversion is generally the most probable, followed by L-shell conversion and so on.

If an assembly of nuclei decays from one excited state to another through N_γ gamma transitions and N_e internal conversion transitions, then

$$\alpha = N_e/N_\gamma \tag{15}$$

is defined to be the internal conversion coefficient. Since the conversion electrons are ejected from different atomic shells, then

$$N_e = N_{e_K} + N_{e_L} + N_{e_M} + \cdots \tag{16}$$

and the conversion coefficient may be defined for the various atomic shells as:

$$\alpha = \alpha_K + \alpha_L + \alpha_M + \ldots \tag{17}$$

where $\alpha_K = N_{e_K}/N_\gamma$ is the K-shell conversion coefficient

$\alpha_L = N_{e_L}/N_\gamma$ is the L-shell conversion coefficient,

and so on. Extensive theoretical calculations of internal conversion coefficients have been undertaken and tabulated by Rose.[6]

Certain general statements concerning the nature of

internal conversion coefficients as theoretically predicted may be listed as follows:

(a) α increases with increasing Z and L and decreasing transition energy.

(b) For a given transition energy and Z, $\alpha_{el} > \alpha_{mag}$.

(c) α_K/α_L decreases with increasing L for given Z and transition energy.

(d) $(\alpha_K/\alpha_L)_{el} < (\alpha_K/\alpha_L)_{mag}$ for a given L, Z and transition energy.

Thus the internal conversion coefficient is a very useful measure of the spin and parity changes associated with a nuclear transition.

V. Methods of Measurement in Nuclear Spectroscopy

Many experimental techniques have been devised for the study of nuclear radiations, some of which have suggested themselves through theoretical considerations. The development of the scintillation counter and advances in photomultiplier design have been basic to the improvements achieved in gamma-ray spectroscopy. The same may be said for associated electronic circuitry and in particular for the refinements made in coincidence techniques. In the field of beta spectroscopy, the improvements have been

mostly in spectrometer design and one such improvement is the subject of part of this thesis.

Within the current structure of nuclear theory, the general aim of nuclear spectroscopy in the study of a particular nucleus, is to establish the energy sequence of the excited states of the nucleus and to measure the energy, spin and parity associated with each of these states. There are, of course, other properties which may be assigned to each nuclear state but those mentioned are the ones of primary concern in nuclear spectroscopy.

The two basic tools used in beta- and gamma-ray spectroscopy are the magnetic spectrometer and the scintillation crystal-photomultiplier spectrometer. The two spectrometers operate on contrasting principles.

The magnetic spectrometer will be discussed in detail later, but it is useful to note some of the basic principles at this time. When a charged particle (electron) enters a magnetic field, it experiences a force $\bar{F} = \frac{e}{c} (\bar{v} \times \bar{B})$ and thus describes a trajectory whose characteristics depend upon $\bar{v}$ and $\bar{B}$. It is possible to design magnets whose induction $\bar{B}$ is of such a nature that electrons of a particular velocity $\bar{v}$ are "focussed" after traversing the field $\bar{B}$. Electrons of other velocities are deflected away from the focus. Thus every velocity has a corresponding field strength to achieve a focus. When arrangements are made such that

only the focussed electrons are detected (or counted), then a graph of the intensity versus B gives the intensity distribution of electron momenta. Generally such instruments are characterized by high resolution and low efficiency of detection.

The scintillation spectrometer on the other hand, makes use of the properties of certain crystals. These crystals emit a pulse of light when a charged particle or electromagnetic radiation is absorbed in the crystal. For particle absorption, the intensity of the light pulse produced is roughly proportional to the energy of the incident particle. For gamma-ray absorption, the pulse height output of the crystal is more complicated because of the different modes of energy dissipation for photons in the crystal. Another part of the scintillation spectrometer is the photomultiplier, made up of a light-sensitive cathode and an electron multiplier for light detection. For maximum response it is necessary that the spectral sensitivity of the cathode match the spectrum of the light emitted by the crystal. The measured spectrum of particle energies is simply the resulting pulse height distribution of the photomultiplier output. Generally such spectrometers are characterized by low resolution and high detection efficiencies.

The two types of spectrometers described above may be used singly or in combination in a number of different ways

to obtain useful data. Very briefly, some of the methods used in beta- and gamma-ray spectroscopy are as follows:

(a) Gamma-ray spectrum - The so-called singles gamma-ray scintillation spectrum is sometimes sufficient for the energy determination of the gamma-rays emitted by a particular radioactive nucleus but the inherently poor resolution of scintillation spectrometers makes this a difficult task if the spectrum is at all complex.

(b) Photoelectron spectrum - A more accurate energy determination for gamma-rays is obtained in the photoelectron spectrum using a magnetic spectrometer. This technique utilizes the photoelectric effect by allowing gamma-rays to fall on a thin foil of high Z material such as lead or bismuth and analyzing the ejected photoelectrons. Upon taking into account the binding energy of the atomic states from which the electrons are ejected in the foil and the energy dependence of the photoelectric cross-section, both the transition energies and relative gamma-ray intensities may be determined with considerable accuracy.

(c) Gamma-gamma coincidence spectrum - The coincidence technique, used extensively in gamma-ray spectroscopy, is useful both in establishing the sequence of gamma emissions from a nucleus and in energy determinations through separation of gamma-rays in a coincidence spectrum. Only scintillation spectrometers can be usefully employed with this method.

(d) Gamma-gamma angular correlation - Theory predicts that the angle between two gamma-rays emitted successively, or in cascade, in a system of three nuclear levels depends upon the spins and parities of the levels. That is, if the first gamma-ray in the cascade, γ_1, is emitted in a particular direction $\bar{r}_1$, the probability of emission of the second gamma-ray, γ_2, in the direction $\bar{r}_2$ is a function of the angle between $\bar{r}_1$ and $\bar{r}_2$. The gamma-gamma angular correlation method, using scintillation counters, necessarily employs coincidence techniques and is useful in spin determinations. Theoretical calculations of angular correlations between both pure and mixed transitions have been done by Biedenharn and Rose.[7]

(e) Beta-gamma coincidence spectrum - This method exploits the high resolution of a beta-ray spectrometer and the high transmission available in a gamma-ray scintillation spectrometer. The ordering of transitions is easily established by this method thus facilitating the analysis of a decay scheme. Further information can often be obtained from coincidences between conversion electrons and gamma-rays. This technique is equivalent, in a sense, to the gamma-gamma coincidence technique with one channel of the apparatus having very good resolution.

(f) Beta-ray spectrum - Analysis of a beta-ray spectrum with a magnetic spectrometer gives information about level

energies through end point energy measurements. In cases where the degree of forbiddenness can be determined, information concerning spin and parity changes is also obtained.

(g) Internal conversion spectrum - The internal conversion spectrum is the most accurate method for determining transition energies as it is measured under the conditions of relatively good resolution inherent in beta-ray spectrometers. From this spectrum and from gamma-ray intensity measurements it is possible to calculate conversion coefficients which, if known accurately enough, determine the multipolarities of the transitions.

The absolute determination of the internal conversion coefficient of a transition requires an accurate knowledge of certain geometric parameters of the beta-ray spectrometer being used in the experimental investigation. These parameters are often difficult to measure with sufficient accuracy to reduce the corresponding uncertainty in the calculated internal conversion coefficient. This difficulty can be avoided by measuring the so-called K/L ratio, or the ratio of intensities of the K-shell conversion electrons to the L-shell conversion electrons. Unfortunately, this method is not as useful as was originally anticipated because of the experimental difficulty of measuring the L-shell conversion intensity coupled with the relative insensitivity of the K/L ratio to the type of multipole radiation. The use of

refined techniques to measure the beta-ray spectrometer geometric parameters can, however, overcome this problem to a large extent.

An interesting case is the $0 \longrightarrow 0$ transition where selection rules forbid an electromagnetic transition. Thus only internal conversion can occur and the associated internal conversion coefficient is therefore infinite.

VI. Beta-ray Spectrometers

a) Instrument Parameters

There are various parameters which characterize the focusing properties of a magnetic beta-ray spectrometer. The two parameters most descriptive of spectrometer performance are transmission and resolving power. Resolving power is a measure of the spherical aberration of the instrument and is defined in terms of how this aberration affects the shape of the spectrum of a radioactive source of monoenergetic electrons. In practise, this is accomplished by examining an internal conversion line in a spectrum. The most common definition of resolving power is $R = \frac{p}{\Delta p}$, where p is the momentum of the electrons producing the conversion line and Δp is the line width measured at half intensity. It has become customary to refer to the quantity $\frac{\Delta p}{p}$ as the

"resolution" of the instrument but in this thesis $\frac{\Delta p}{p}$ will be called simply the line width and will be expressed as a percentage.

Beta-rays are emitted, of course, by the source into 4π steradians but only a small fraction of them are detected. This fraction is defined to be the transmission, T. A related parameter is the gathering power, ω, which is defined to be the fraction of 4π steradians subtended by the entrance baffles at the source. In other words, the entrance baffles make available for magnetic analysis and detection by the spectrometer those beta-rays emitted by the source into a solid angle of $4\pi \cdot \omega$ steradians. Unfortunately, all beta-rays passed by the source-entrance baffle system for magnetic analysis are not necessarily focused. This means that $T \leq \omega$.

In some applications, other parameters are also useful in describing instrument performance. Two examples of these are the dispersion and luminosity parameters. Dispersion, D, is defined as $D = \frac{dx}{d(H\rho)}$, where x is a suitable coordinate defining the position of the focus and $H\rho$ is the electron momentum in gauss-cm. This parameter is a measure of the ability of the instrument to separate adjacent lines in a spectrum.

In order to obtain a good spectrum, the source must be kept thin to reduce scattering within the source itself. Thus, to obtain sufficient activity, source material of high

specific activity is usually required, particularly if the source must also be small. In cases where this is not possible and an extended source has to be used to obtain the required activity, the luminosity parameter, Λ, measures the ability of a spectrometer to make use of an extended source. Luminosity is defined as $\Lambda = \sigma \cdot \omega$, where σ is the area of the source and ω is the gathering power. A more meaningful parameter in practice is the "overall luminosity", L, defined to be $L = \sigma \cdot T$. From the relationship between ω and T, it is clear that $L \leq \Lambda$.

As far as transmission and resolving power are concerned, one obviously wishes to have an instrument with high transmission and high resolving power. In a particular application, it is often desirable to optimize either the transmission or the resolving power at the expense of the other. For example, a complex spectrum requires an instrument with high resolving power to separate the various internal conversion lines whereas a low activity source requires a high transmission instrument to keep the counting time down to a reasonable level.

b) Types of Instruments

Gerholm[8] has written an extensive article dealing with beta-ray spectrometers, so only a brief account of the various types of spectrometers will be given here for the

sake of completeness. The one exception to this will be the thin-lens spectrometer, a modification of which is discussed later.

Beta-ray spectrometers may be very generally divided into magnetic focusing instruments which are momentum selective and electrostatic focusing instruments which are energy selective. The latter type is rarely used mainly because it is limited by the range of electron energies that can be focused. The production and control of the very large electric fields required involve technical problems difficult to overcome. By comparison, a magnetic field of 1000 gauss produces the same radius of curvature as an electric field of 300,000 volts/cm. Thus, the beta-ray spectrometers in use today are almost without exception those of the magnetic focusing type.

Magnetic focusing spectrometers may be further classified into the so-called flat spectrometers and the helical, or lens-type spectrometers, the distinction being that the electron trajectories in the former type lie in planes approximately perpendicular to the magnetic axis while electron trajectories in the lens-type spectrometer lie in planes that contain the magnetic axis. The phrase "planes that contain the magnetic axis" should really read "rotating planes that contain the magnetic axis" because the electrons in the lens-type spectrometer follow helical trajectories

over part of the source-detector distance.

i) Flat spectrometers

Great improvements have been made over the years in the properties of flat spectrometers, chiefly by shaping the magnetic field. One such improvement utilizes the third-order focusing principle illustrated in Fig. 1 wherein all electrons emitted in the same plane are focused at the same point. A further improvement employs double focusing, as in Fig. 2, in which the electrons are focused in both the horizontal and vertical directions. Variations on the flat spectrometer design are the so-called prism and sector field spectrometers in which both source and detector are outside the region of the magnetic field, as in Fig. 3. In these spectrometers, the shape of the pole pieces where the electrons enter the magnetic field is a variable which permits the optimization of particular desired properties. A novel design, in Fig. 4, effectively employing six sector-field spectrometers in parallel, is the "orange" spectrometer of Kofoed-Hansen, Lindhard and Nielson.[9]

ii) Helical spectrometers

As in the case of flat spectrometers, several characteristic types are definable in the family of helical spectrometers. The solenoidal spectrometer employs a uniform magnetic field over the entire electron path, thus lending itself to simple computation of electron trajectories.

To follow page 27

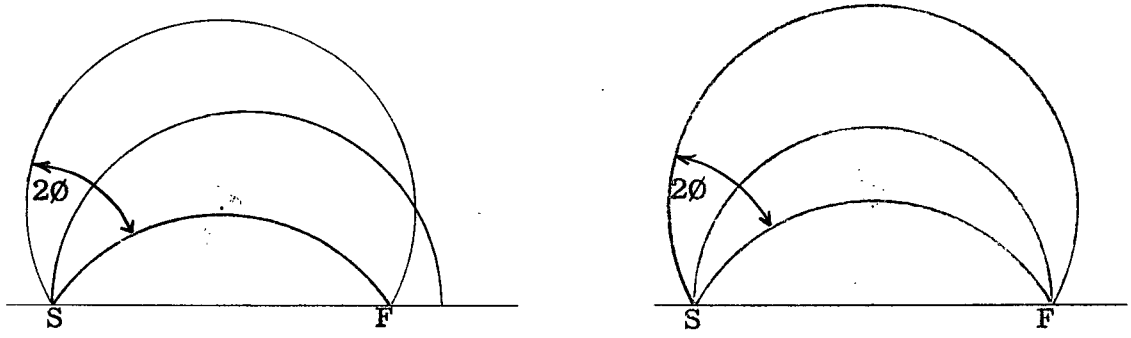

Figure 1 - Third-order focusing principle.

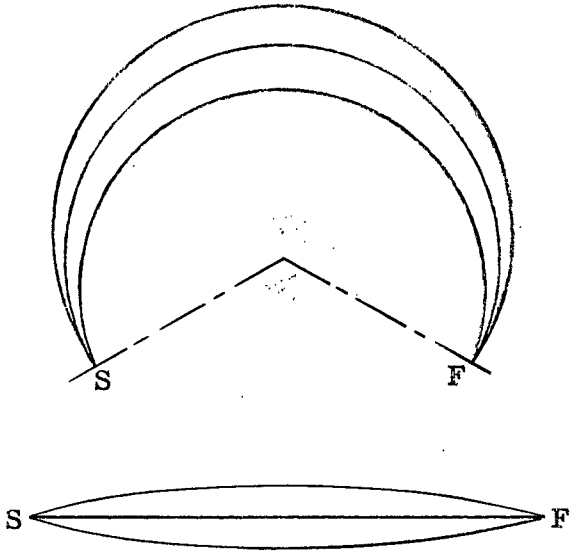

Figure 2 - Double focusing principle.

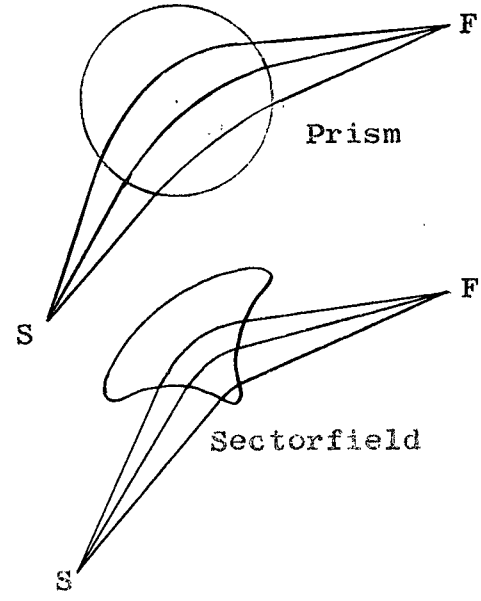

Figure 3 - Sectorfield and prism spectrometers.

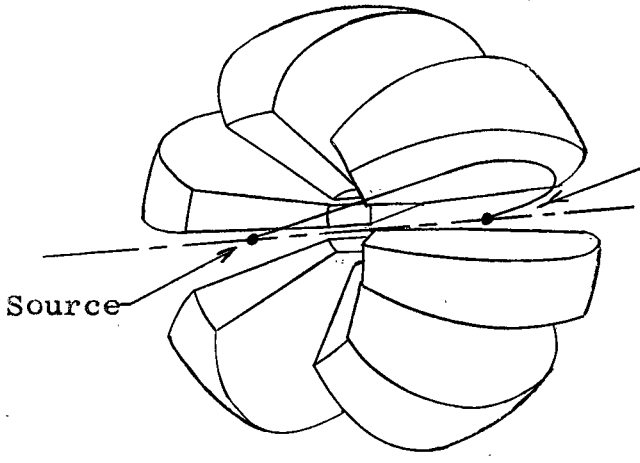

Figure 4 - "Orange" spectrometer.

Theoretical calculations have been made to determine the magnetic field shape required to reduce the inherent focusing aberrations. Such a field shape is approximated in the long-lens spectrometer and the intermediate-image spectrometer. Both of these spectrometers have the source and detector in regions of strong magnetic field. For some applications, this factor limits the flexibility of use of the spectrometer.

One further type of helical spectrometer is the thin-lens type. It is characterized by an inherently large spherical aberration but a modification to reduce this limitation can be very simply incorporated into the instrument. Such a modification will now be discussed.

CHAPTER II

RING FOCUS COLLECTION IN A THIN-LENS MAGNETIC SPECTROMETER

I. Introduction

While the thin-lens spectrometer does not exhibit either the high transmission or the resolving power that can be attained with various other instruments now available, it does possess some attributes which are worth discussing here. It is an inexpensive instrument both to operate and construct. This, of course, derives partly from the fact that the power requirements are small and the associated control circuits are few. It is also a mechanically simple instrument employing only a vacuum chamber and an air-core magnet.

The thin-lens spectrometer in this laboratory, as originally used, exhibited only a moderate transmission ($\backsim$ 0.4%) and resolution (line width $\backsim$ 3.0%). These performance characteristics are poor enough to set serious limits on the usefulness of the instrument, particularly in the analysis of complex decay schemes. Therefore, an investigation into the possibility of improving the instrument was

undertaken.

For many years it was known that magnetic lens-type spectrometers displayed a "ring focus" of electron trajectories, as in Fig. 5, somewhat analogous to the "circle of least confusion" in an optical lens system. This spherical aberration effect, and the effect of other aberrations, was reduced by using a symmetric geometry in which the source and detector were placed equal distances from the magnet on the magnetic axis. On the other hand, several workers[10-13] have taken advantage of the ring focus property by placing baffles at the position of the ring focus, resulting in an improvement of the instrument performance. In once case[11], the transmission was calculated to increase by a factor two for a given resolving power.

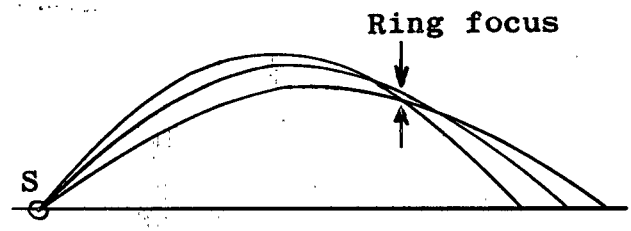

Figure 5 - Electron trajectories in a helical spectrometer.

In an instrument of this type, the electron trajectories at the position of the ring focus are diverging and therefore cross the magnetic axis at widely separated points. This makes it difficult to collect all the electrons with an axial detector unless the spread in emergent angle of electrons from the source is kept small, thus reducing the transmission.

The modification to the instrument in this laboratory improved its transmission in two ways. First, the detector was placed at the position of the ring focus so that all electrons passing through the ring focus were collected. Second, an assymmetric geometry was used in which the source to magnet distance was decreased to allow the use of trajectories having larger emergent angles. That is, the symmetric geometry of the unmodified instrument limited the maximum emergent angle at the source because of the finite size of the vacuum chamber. By moving the source closer to the magnet, emergent angles in the region of greater geometric acceptance became available and a larger transmission was attained.

II. Preliminary Investigation

A series of trajectories were calculated for us by the Computation Center at the McLennan Laboratory, University of Toronto to determine where the ring focus was located and what degree of assymmetry could be employed. These calculations were based upon the method of Deutsch, Elliott and Evans[14] and used the following equations:

The equation defining the electron trajectories was:

$$r'' \frac{(k^2-A^2)}{(1+r'^2)} - r'A \frac{\partial A}{\partial Z} + A \frac{\partial A}{\partial r} = 0$$

where A is the vector potential per ampere of magnetizing current

r is the radial displacement

z is the axial displacement

k is the electron momentum in gauss-cm/ampere

r' and r" are time derivatives.

The vector potential A is calculated from the equation:

$$A(r,z) = \frac{r}{2} H_o(z) - \frac{r^3}{16} \frac{\partial^2}{\partial z^2} H_o(z) + \frac{r^5}{384} \frac{\partial^4}{\partial z^4} H_o(z) - \ldots$$

where $H_o(z)$ is the axial magnetic field given by:

$$H_o(z) = \frac{2n\pi}{10L(a_2-a_1)} \left\{B(a_2)-B(a_1)\right\}$$

in which, n is the number of turns in the magnet = 2040

a_1 is the inner radius of the magnet = 11.02 cm.

a_2 is the outer radius of the magnet = 28.40 cm.

L is the axial length of the magnet = 17.61 cm.

and the function B is given by:

$$B(a) = (z+\tfrac{L}{2}) \ln\left\{a+\left[a^2+(z+\tfrac{L}{2})^2\right]^{1/2}\right\} - (z-\tfrac{L}{2})\ln\left\{a+\left[a^2+(z-\tfrac{L}{2})^2\right]^{1/2}\right\}$$

It is at once apparent that there are many parameters that determine the nature and position of the ring focus, and to optimize completely the performance of the instrument, each parameter would have to be indepentently adjustable. These parameters are:

(a) source-to-magnet distance,

(b) the spread of emergent angles accepted from the source,

(c) ring detector-to-magnet distance,

(d) ring detector radius, and

(e) ring detector slot width.

Independent adjustment of each of these variables poses a formidable mechanical problem, since all adjustments have to be made in vacuo. Therefore a compromise was adopted. The source-to-detector distance (limited by the available tube length) was fixed at 69.7 cm. Simultaneous variation in (a) and (c) above was obtained by sliding the tube axially through the focusing magnet. The mean ring detector radius was kept fixed at about 5 cm. Parameters (b) and (e) were altered manually by the use of a set of appropriate baffles of slightly different radii.

These restrictions are illustrated in Fig. 6, taken from the calculated trajectories, in which the radial displacements of trajectories in the plane of the ring focus are plotted as a function of emergent angle. For the case illustrated, the mean emergent angle has a tangent of about 0.32 and the gathering power is 1.10%. This choice of entrance baffles produces a ring focus about 1 mm wide at a mean radius of 5.15 cm. It is apparent from the figure that for a given source position there is

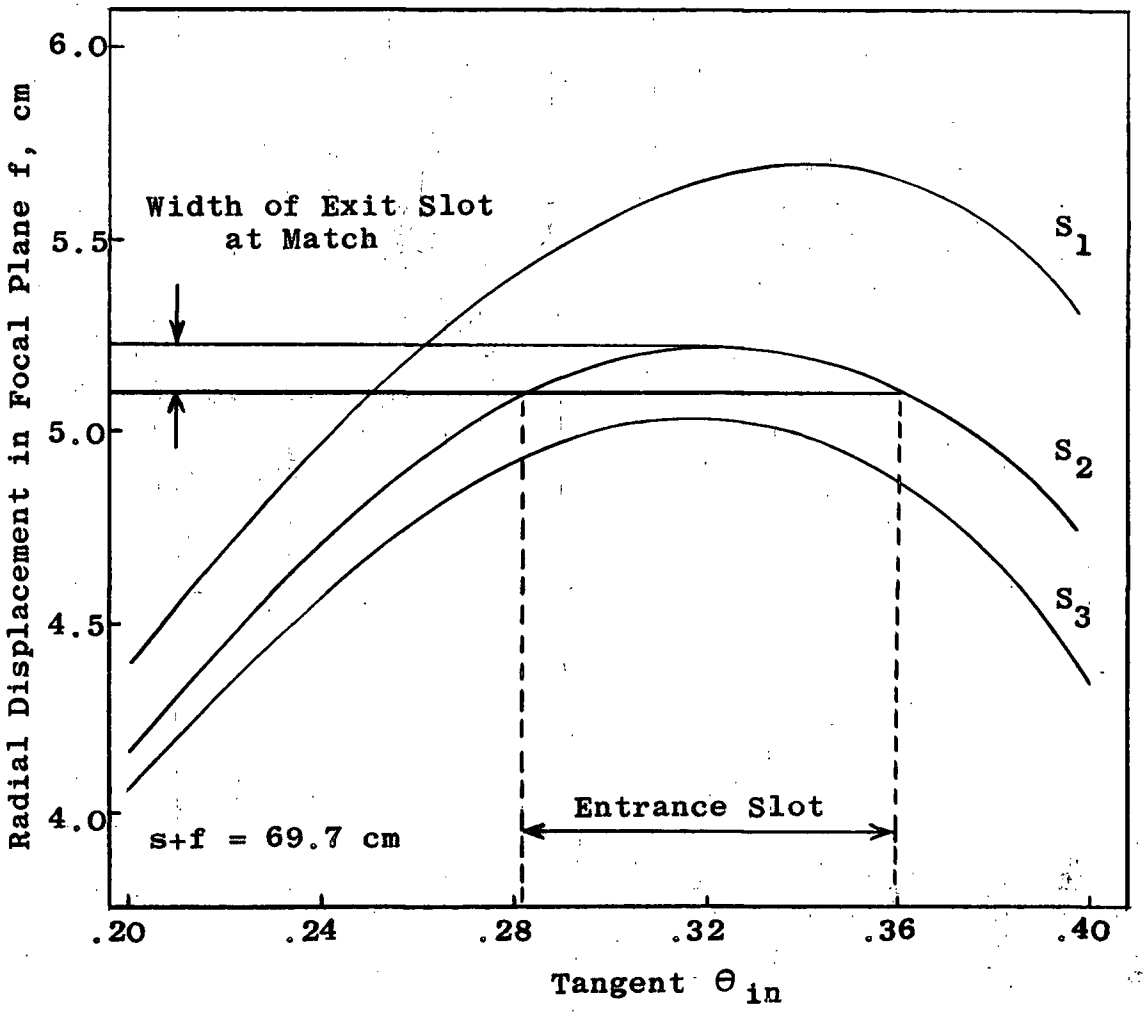

Figure 6 - Graph illustrating the match of the ring focus exit slot for a given entrance slot.

a unique pair of emergent angles which define a ring focus of a given width.

It should be noted here that the instrument displays optimum performance when the width of the trajectory envelope at the ring focus and the width of the annular exit aperture are equal. This condition will be referred to as

a "match". If the condition of a match does not exist and the exit
/slot is too wide, then the resolving power of the instrument is determined by the slot width. In this case, the slot width is reduced in steps. With each step, the line width decreases with no loss of transmission until the peak height begins to decrease. This point represents a match. Conversely, if the exit slot is too narrow, the resolving power is determined by the width of the trajectory envelope at the ring focus. The slot is then opened in steps to increase the transmission, with no change in line width, until the match condition is reached.

Fig. 6, in addition to indicating the optimum slot width for a given pair of source baffles, also indicates the optimum mean radius of the exit slot. Ideally, this means that the exit slot should be of variable mean radius as well as variable width. A few tests showed, however, that the instrument performance was very insensitive to change in this parameter. Theoretically, this means that the instrument constant k (gauss-cm/ampere) has been slightly decreased while the character of the focus itself is practically unchanged. Based upon the above considerations, the radius of the outer exit baffle was made 5 cm and the inner exit baffle was changed to vary the width of the exit slot, the effect of the slight change in mean radius being negligible.

III. The Modified Thin-Lens Spectrometer and Associated Apparatus

a) General mechanical description

A schematic drawing of the spectrometer used in this laboratory is shown in Fig. 7. The vacuum chamber is constructed of 1/8" brass tubing, is 1 meter long and has an outer diameter of 8". The magnet is made of four coils of No. 8 gauge formex magnet wire each containing about 510 turns and separated from each other by cooling coils. The width of the magnet spool is approximately 8 1/4" and the inner and outer diameters of the spool are 8 1/2" and 24" respectively. Compensation coils are used to cancel the vertical component of the earth's magnetic field.

Accurate centering of the source is essential whenever narrow exit slots are used or when the source is small in size (i.e. < 2 mm diameter). The source-centering mechanism allows the source to be positioned in the plane which contains the source and which is perpendicular to the axis of the vacuum chamber. It is a simple rack and pinion arrangement and is operated by control rods passing through vacuum seals in the end plate at the source end of the spectrometer.

The entrance baffles are made from 1/8" aluminum sheet and are mounted on standoffs about 4 cm in front of the source in such a way as to move rigidly with the source.

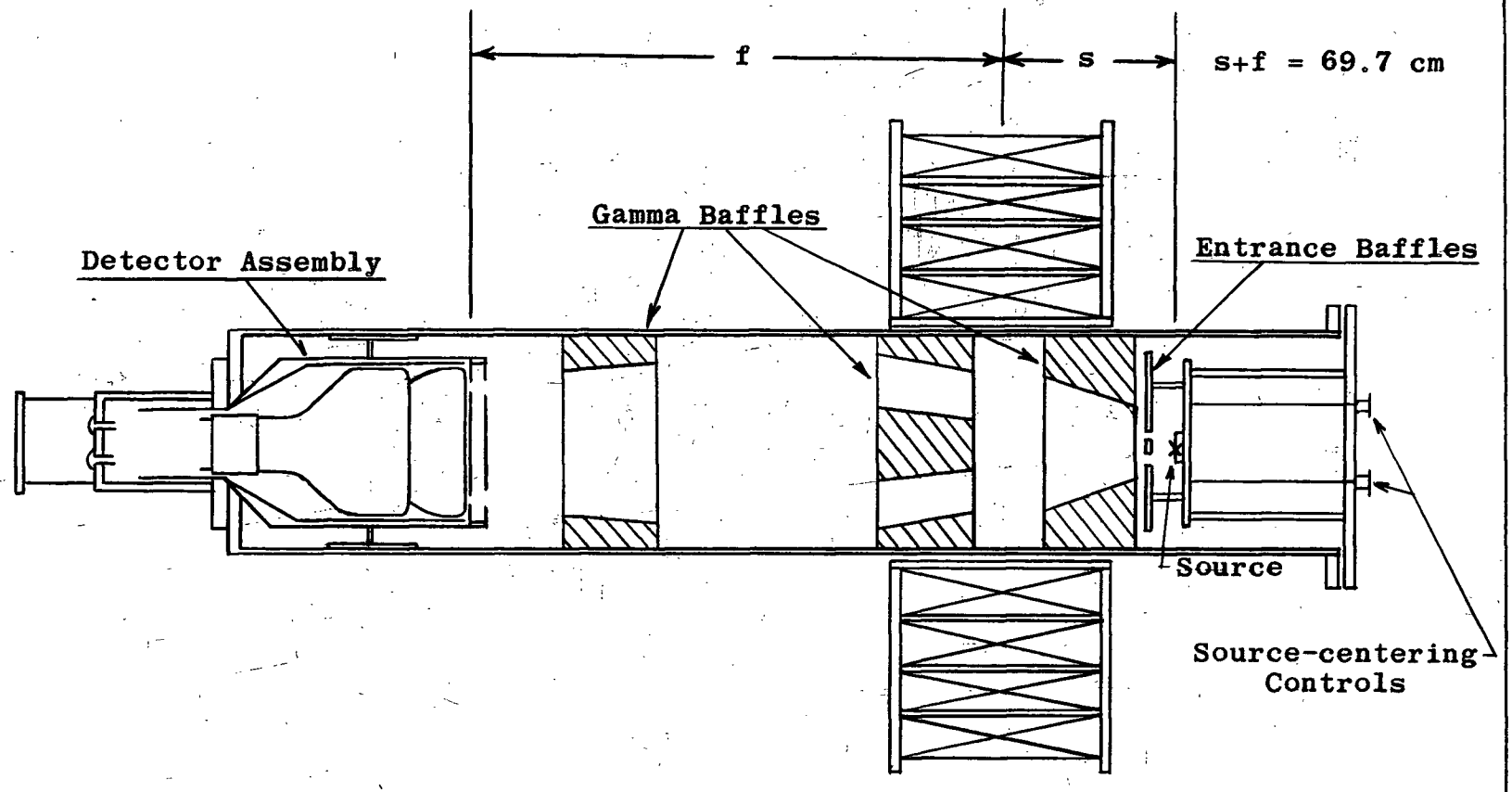

Figure 7 - The modified thin-lens spectrometer.

To follow page 36

A lead baffle is situated in the chamber to shield the detector from direct gamma radiation from the source. Other lead baffles are placed in the vacuum chamber to diminish the number of scattered electrons and photons that reach the detector when an intense source is used.

The whole of the detector is located inside the vacuum chamber and as a result care has to be taken that the vacuum is "hard" enough to prevent electrical discharge in the bleeder supplying the dynode voltages to the detector. Voltage supply leads and signal leads are fed into the vacuum chamber through three Kovar seals in the end plate at the detector end of the instrument.

b) The detector

A major modification necessary to improve the performance of the thin-lens spectrometer was the design and construction of a detector able to collect electrons at the position of the ring focus. The detector currently being used is one of many that have been tried, the first of which was built by J. A. L. Thompson in this laboratory in 1953. It consisted of a lucite light-cone arrangement which conducted the light from the scintillator, set into the periphery of the light-cone, onto the face of a 2" photomultiplier. Milley[15] improved the design of the light-cone by calculating the surface shape necessary to produce

critical internal reflection.

During the current investigation, several detector designs were assembled and tested. The first of these embodied a further improved light-cone coupled to an EMI 6262, a 14-stage 2" photomultiplier. A plastic scintillator was employed in this detector which was the one used to determine the sensitivity of the ring focus width to the mean radius of the exit slot.

At this point in the investigation 5" photomultipliers became available commercially and three Dumont 6364 photomultipliers were purchased. Difficulties had been encountered with optical coupling at the crystal-lucite and lucite-photomultiplier interfaces, and for this reason a detector was tested that consisted simply of a ring of plastic scintillator glued onto the face of a Dumont 6364 with R313*. This detector proved to have a poor signal-to-noise ratio which was thought to arise from the low sensitivity of the photocathode of the 6364 at its edge. Subsequent investigation into the sensitivity of the photocathode of a 6364 showed that the peak sensitivity at the center of the photocathode could be several times larger than at the edge. The sensitivity pattern also varied with different photomultipliers and was found to be markedly dependent on the voltages

---

* Available from Carl H. Biggs Co., Los Angeles, Cal.

applied to the dynodes and the focusing electrode.

The above considerations indicated that a light pipe arrangement had to be used to allow scintillation photons to fall on the center portion of the photocathode where the sensitivity was greatest. Various light-pipe designs were tested, the best being the one shown in Fig. 8. It is designed for critical internal reflection at the surface and has a diameter, at the lucite-photomultiplier interface, equal to the diameter of the photocathode. The surface of the light-pipe is covered with aluminum foil to contain any light that may be transmitted rather than reflected. Finally, the light-pipe is held centered over the photocathode by means of a bakelite ring which is fixed onto the face of the photomultiplier with Armstrong cement.

The scintillator used in this detector is anthracene. Tests showed that the pulse output of the plastic scintillator NE 101 was only about one-third that of anthracene.

Various optical coupling materials were tested. At the lucite-photomultiplier interface it was difficult to produce a long lasting coupling with silicone oil. Even when using the very high viscosity DC200 fluid it was found that this oil gradually drained away from the interface. To remedy this situation, a silicone gum (DC400) was tried but was found very difficult to spread into a thin layer. By diluting the gum with the oil it became possible to produce a

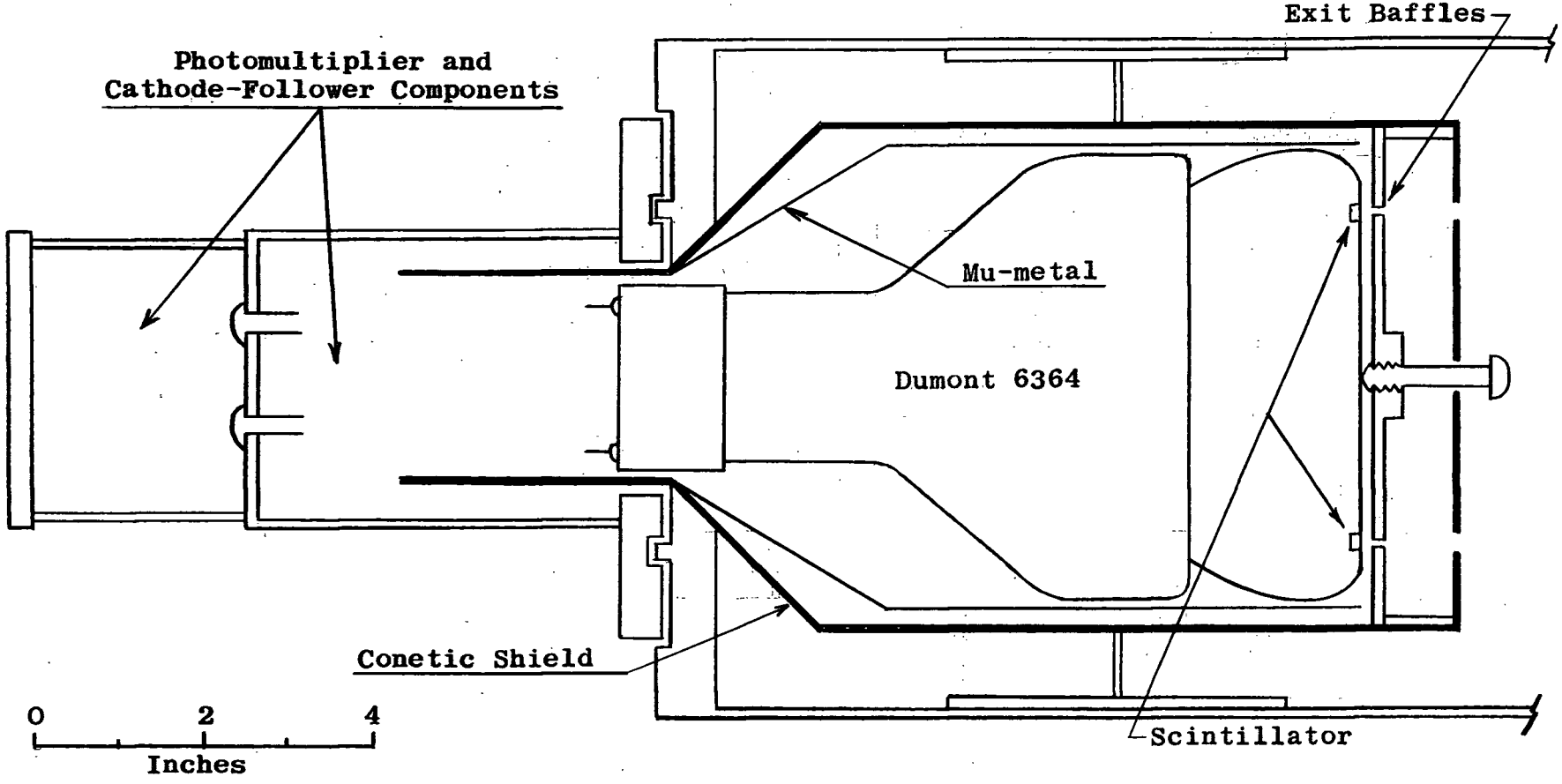

Figure 8 - The detector assembly.

To follow page 39

thin layer of coupling fluid that would not flow. A different material is used to couple the anthracene crystals to the lucite. The oil, gum and oil-gum mixture were found to be inadequate at the crystal-lucite interface as they generally contained minute air bubbles which expanded under vacuum lifting the crystals out of their slot. While the air did eventually dissipate, it required considerable time to do so and therefore other coupling materials were tried. It was decided to use a mixture of glycerine and Ivory soap for a coupling material. This mixture, the preparation of which is described by Fleishman et al[16], flows readily when warm but is solid at room temperature. These properties allow easy installation of the anthracene crystals and eliminate the air bubble problem.

While the detector is removed a reasonable distance from the magnet, a sufficiently intense residual magnetic field can exist, even at this distance, to cause defocusing of the photoelectrons within the photomultiplier. It is necessary, therefore, to incorporate a magnetic shield into the detector assembly. The magnetic shield, seen in Fig. 8, is actually constructed of two shields, both of which are commercially available. The outer shield is a Fernetic-Conetic* shield specifically designed for 5" photomultipliers

---

* Available from Perfection Mica Co., Chicago, Illinois.

and the inner shield, made of mu-metal, is also a standard shield for 5" photomultipliers. The face plate of the outer shield was made in this laboratory from Fernetic and Conetic sheet material and was magnetically coupled to the rest of the outer shield by an iron ring. Fig. 9 illustrates a check on the efficiency of the magnetic shielding that was carried out by measuring the variation in background counting rate with magnetic field.

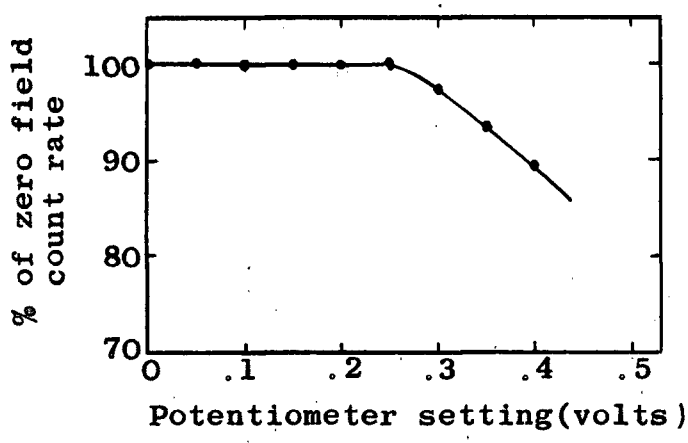

Figure 9 - Defocusing effect on photomultiplier noise.

The exit baffles are made of 1/8" aluminum sheet and are mounted directly in front of the anthracene crystals. The inner exit baffle is held rigidly to the outer exit baffle by a spider leg arrangement connecting the two and the whole assembly mounted on the back of the iron ring mentioned above. A tapped hole in the center of the inner exit baffle and a hole in the face plate of the magnetic shield allow the introduction of a machine bolt to keep the light-cone pressed against the face of the photomultiplier and also to keep the crystals rigidly centered behind the exit slot.

c) <u>The electronics</u>

The investigation of the focusing properties of the

modified thin-lens spectrometer requires only the standard electronics associated with any beta ray spectrometer.

i) The control circuit

The electric current used to produce the focusing magnetic field was provided by a 110 V d.c. source. As shown in Fig. 10, the current passed through a series circuit consisting of the magnet, a bank of 38 6AS7's connected in parallel and a 0.1 ohm standard resistance made of manganin. This circuit was designed to handle currents up to 10 amperes. A Rubicon potentiometer supplied an accurately known voltage with which the voltage developed across the standard resistance by the magnet current was compared. This comparison was carried out in the bias control circuit which fed the required bias onto the grids of the 6AS7's. The sensitivity of the bias control circuit was 1 part in 10^4. This sensitivity was achieved using an a.c. amplifier of frequency response from 10 c/s to 2000 c/s and a gain of 10,000 coupled with a Brown converter-fed d.c. control amplifier having a frequency

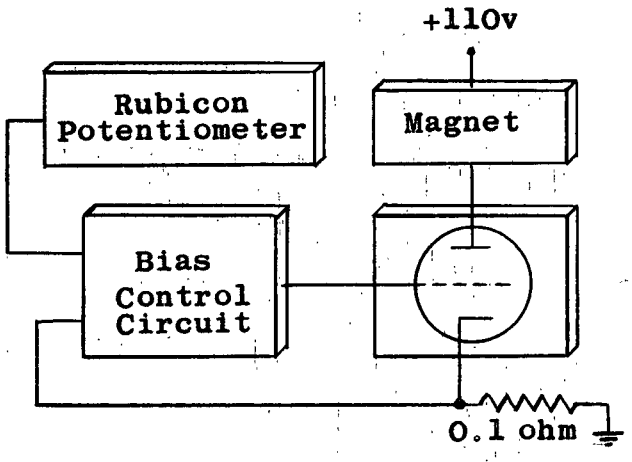

Figure 10 - Control circuit

response from 0 c/s to 20 c/s and a gain of 30,000.

ii) Beta spectra counting circuit

In the counting circuit, shown in Fig. 11, the collector output of the photomultiplier fed a 6J6 cathode follower used to match the impedence of the signal cable. The pulses were then amplified by a Tracerlab amplifier, model RLA-1, and fed to a scalar. The scalar used was a standard scale of 64 scalar, model 101-M, available from Atomic Instruments Corporation. High voltage for the photomultiplier was provided by a TMC model HV-4A power supply.

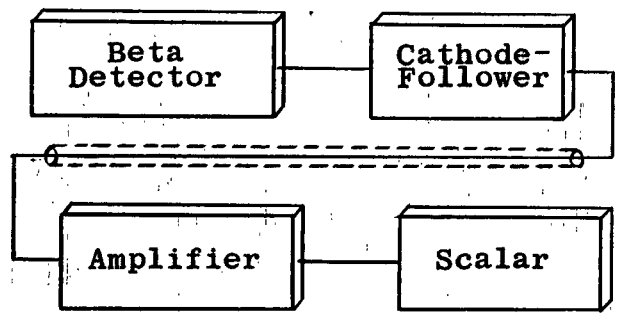

Figure 11 - Counting circuit

All dynodes of the photomultiplier were supplied voltage from a bleeder made up of 500 KΩ resistors except for the 1st dynode stage which contained a 2MΩ potentiometer. The tap point on the potentiometer supplied the focusing screen voltage for the photomultiplier and with an H.T. of 1350 V the optimum screen voltage was found to be 2.6 V above the photocathode.

IV. Experimental Investigation of Spectrometer Modification

a) Preliminary procedures

The source used throughout the investigation of the focusing properties of the thin-lens spectrometer using ring focus detection was Cs 137. It contains an isolated internal conversion line of momentum 3381.28 gauss-cm (corresponding to the K-conversion line of the 662 kev transition) making it ideal for this study. The source was obtained from Chalk River and was in the chemical form of $CsNO_3$ dissolved in HNO_3. A beta source was prepared by depositing a drop of the solution on a thin (240 ugm/cm^2) aluminum foil, allowing it to evaporate to dryness and then covering it with a thin film of collodion to contain the active material.

Two procedures that have to be carried out prior to the measurement of any spectrum with this spectrometer are source-centering and setting the discriminator voltage on the discriminator circuit. Source-centering is accomplished simply by recording the variation in peak height of an internal conversion line as a function of source position. This maximizing procedure apparently serves to bring the ring focus into coincidence with the exit slot, but does not, in general, necessarily bring the magnetic axis into coincidence with the source-detector axis. The latter condition is of course the most desirable one but with the source diameters used, the small deviations from it produce only second order

effects which are within experimental error.

For all practical purposes, electrons of a given momentum give rise to a finite spread of voltage pulse heights about some mean value. Thus, all signal pulses lie above a particular voltage level and it is sufficient to count only those pulses which lie above this level thereby rejecting the noise pulses of lesser amplitude in voltage. In practice, the discriminating voltage is determined by measuring the peak height of an internal conversion line as a function of discriminator setting. As the discriminator voltage is decreased to "dig" out more signal pulses, the peak height of the conversion line measured above background increases to some maximum value and further lowering of the discriminator setting does not affect the significant peak height. The graph of peak height versus discriminator setting is thus a plateau-shaped function, the knee of which determines the discriminator voltage setting to be used at the energy of the electrons being focused. If electrons of greater energy are focused on the detector, they of course generate pulses of larger amplitude and therefore the same discriminator setting allows the detection of all of these electrons. For electrons of sufficiently greater energy, however, the discriminator setting may be raised without loss of signal pulses to decrease the background count rate. Thus the discriminator setting established at a particular momentum, p_o, is used

only for the momentum interval (p_o, $p_o + \Delta p$) and then changed to a more advantageous setting. The useful interval Δp decreases with decreasing electron energy.

b) Experimental measurements and results

The three gathering powers of 0.7%, 1.1% and 1.6% were arbitrarily chosen as representative of those to be used in future experimentation for the investigation of the focusing properties of the modified spectrometer. Three mean emergent angles were also chosen for study and source baffles were made to define the previously mentioned gathering powers at these three angles.

With each of the nine possible combinations of gathering power and mean emergent angle, the source position, s, was optimized. This was accomplished by measuring the change in line width and peak height of the Cs 137 conversion line as the vacuum chamber was moved along its axis. A typical run of this type is shown in Fig. 12 in which the line width and peak height are both optimized for the same source position. Physically this means that for this particular source position, the width of the trajectory envelope at the ring focus is a minimum.

The next step in the procedure was to vary the size of the exit slot until a match was achieved. This was done by starting with a very wide exit slot, thus ensuring that all

To follow page 46

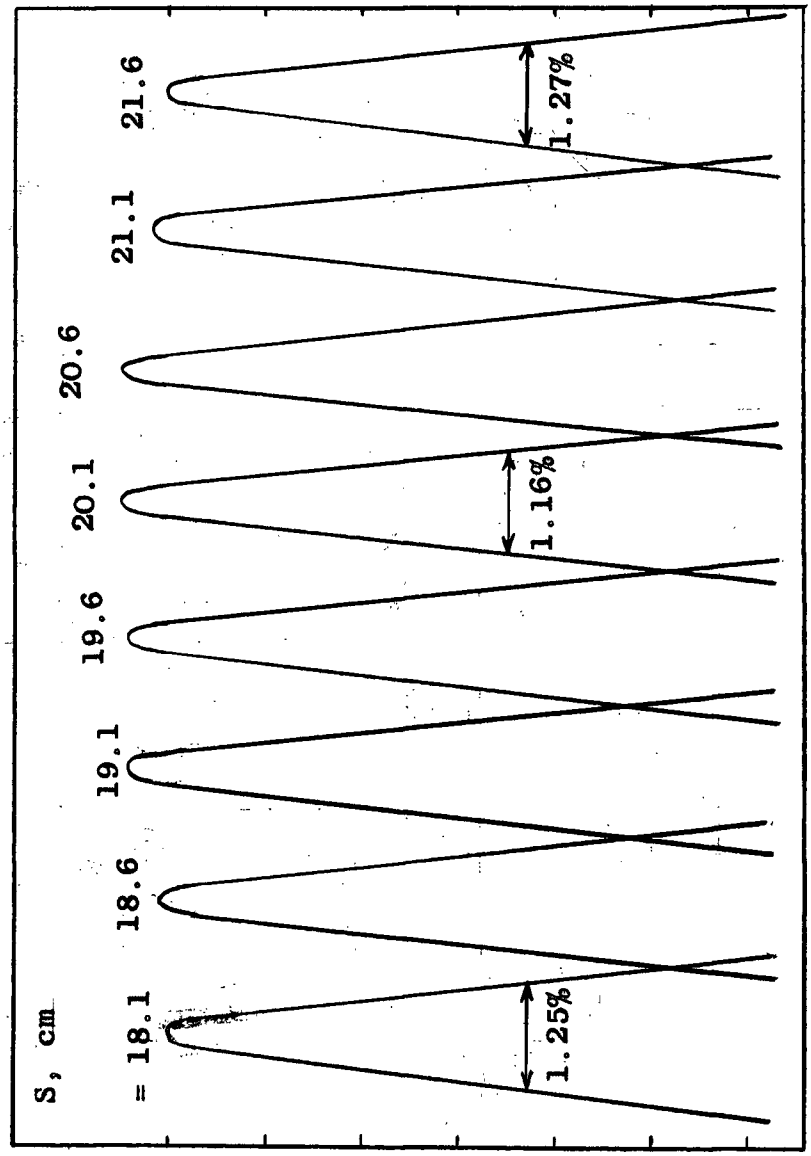

Figure 12 - Effect of source position, s, on peak shape with the restriction s+f = 69.7 cm. Entrance baffles: arctan 0.377 - 0.420 (ω=0.7%); exit slot width = 3.5 mm.

electrons in the ring focus were passing through the exit slot, and then decreasing the slot width in steps until the peak height began to diminish. During this procedure the line width decreased up to the point where the peak height began to drop whereupon the line width then remained constant. The results of the matching procedure seem to support the interpretation, previously outlined, as to the physical nature of the ring focus. The effect on the conversion line of Cs 137 during such a matching procedure is illustrated in Fig. 13.

A summary of the results of the investigation is given

Table I. Summary of results of ring focus collection in a thin-lens beta ray spectrometer taken at three gathering powers with three different mean emission angles. Large source diameter = 2.4 mm, small source diameter = 1.6 mm.

		Line width (%)		Exit slot width (mm)	
ω(%)	Mean tangent	Large source	Small source	Large source	Small source
1.60	0.400	1.54	1.37	3.50	3.25
	0.384	1.54	1.36	3.50	3.50
	0.351	1.59	1.38	3.75	3.50
1.10	0.400	1.30	1.24	3.25	3.25
	0.385	1.31		3.05	
	0.352	1.24		2.90	
0.70	0.399	1.15		3.50	
	0.383	1.09	1.10	3.05	3.05
	0.357	1.19		3.50	

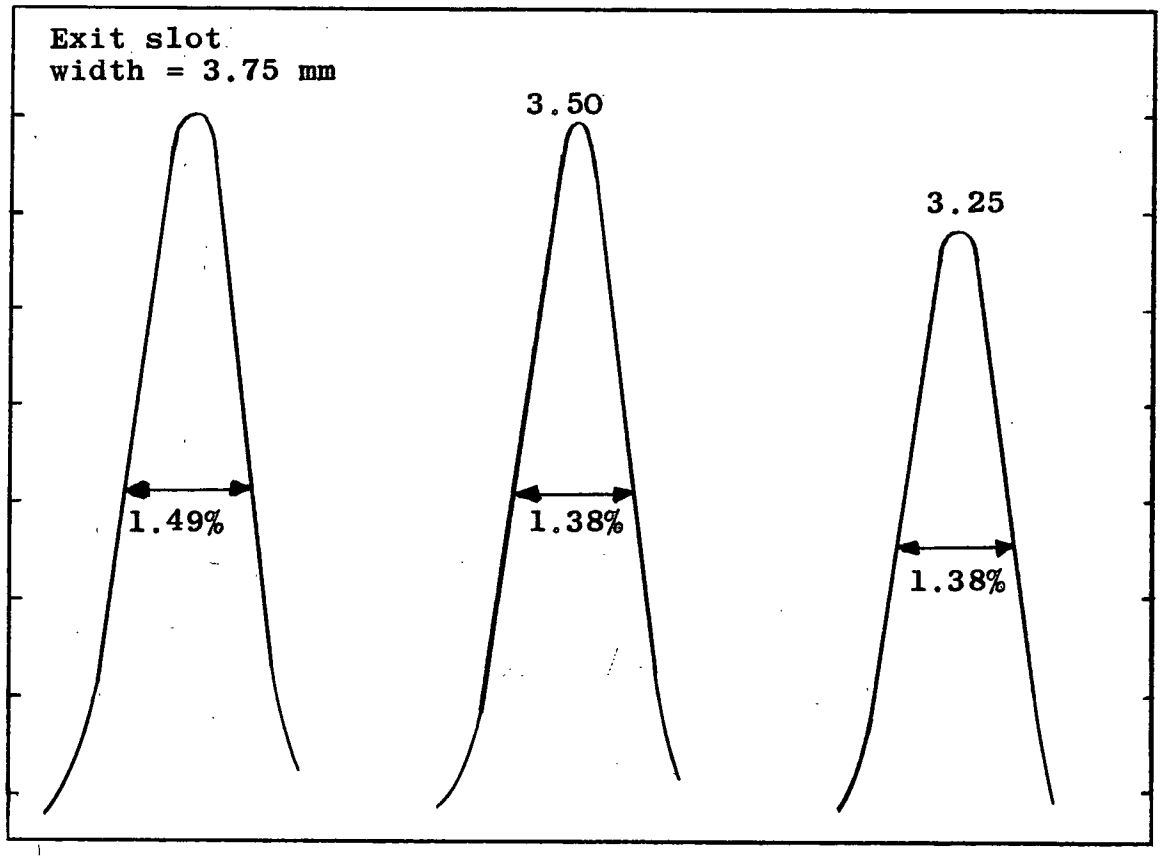

Figure 13 - Effect of exit slot width on peak shape.
Entrance baffles: 0.296 - 0.406 (ω=1.6%).

To follow page 47

in Table I. As may be seen from the table, two sources were used during the investigation. The first source used was approximately 2.4 mm in diameter. A complete survey of mean emergent angles and gathering powers was carried out with this source. A second source 1.6 mm in diameter was made to determine the effect of source size on instrument performance, although this was not done for all possible geometries. The smaller source displayed a smaller line width than that of the first source by about 10%.

The product ωR is useful as a rough measure of the overall performance of a spectrometer and is listed for the various spectrometers in Table II in which the modified thin-lens spectrometer is compared to some high performance helical spectrometers.

The ring focus collection modification incorporated into the thin-lens spectrometer in this laboratory has improved its performance by a considerable factor making it once again a useful tool in nuclear spectroscopy. This is particularly true in the case of photoelectron spectra and beta-gamma coincidence spectra which require for their measurement an instrument having particular geometric properties in addition to simply good performance. For example, a photoelectron spectrum generally requires the use of an intense source. This is a prohibitive requirement in the many spectrometers which have a considerable amount of

To follow page 48

Table II. Comparison of some high performance helical spectrometers. Most of the data taken from reference 17.

Type	Iron	ω(%)	1/R(%)	ωRx100
Solenoidal[a]	No	2.	0.4	500
Intermediate image[b]	No	4.5	1.6	280
Long lens[c]	Yes	6.3	2.4	262
Solenoidal[d]	Yes	3.	1.2	250
Long lens[e]	Yes	2.7	1.3	208
Intermediate image[f]	Yes	8.	4.	200
Intermediate image[g]	Yes	10.	5.5	180
Long lens[h]	No	11.	9.	122
Thin lens[i]	No	1.6	1.37	118

a. F. Schmidt, Rev. Sci. Instr. 23, 361 (1952).

b. D. Alburger, Rev. Sci. Instr. 27, 991 (1956).

c. H. de Ward, Thesis, Groningen University, 1954.

d. T. Gerholm, Rev. Sci. Instr. 26, 1069 (1955).

e. W. Zünti, Helv. Phys. Acta 21, 179 (1948).

f. H. Slätis and K. Siegbahn, Phys. Rev. 75, 1955 (1949).

g. Nichols, Pohm, Talboy, and Jensen, Rev. Sci. Instr. 26, 580 (1955).

h. H. Agnew and H. Anderson, Rev. Sci. Instr. 20, 869 (1949).

i. Present investigation.

scattering material in the region of the source. The modified thin-lens spectrometer is relatively free of scattering material in the region of the source and with its improved performance can now adequately measure photoelectron spectra. Similarly, the measurement of beta-gamma coincidence spectra requires high performance from the beta spectrometer but a difficulty arises with the gamma detector. It is impossible in many spectrometers to incorporate a gamma detector near the source because it is in a region of high magnetic field. This problem is much reduced in the thin-lens spectrometer in which the source does not lie in a high field region. The gamma detector may then be adequately shielded to prevent magnetic defocusing.

Like any other instrument, the modified thin-lens spectrometer has its limitations. One such limitation is the thermal noise of the photomultiplier used in the detector assembly. This reduces the low energy efficiency of the detector since large background counting rates have to be accepted in counting the low voltage pulses. The high energy efficiency of the present detector is indirectly limited through magnetic defocusing in the photomultiplier. Although the photomultiplier is completely enclosed by a magnetic shield, its large size makes it susceptible to defocusing by weak magnetic fields. The defocusing effect can be measured and corrected for, but for sufficiently large magnetic fields

it cannot be tolerated any further. Thus, while the present detector is useful for counting electrons up to $\backsim$ 800 kev without excessive corrections, an improvement in the performance of the instrument could be made through reduction of the defocusing effect. This may be achieved by: (a) moving the detector farther from the magnet, (b) improved magnetic shielding, and (c) using a smaller photomultiplier. The use of a smaller photomultiplier would reduce both the shielding problem and the problem of thermal noise.

In spite of these limitations on the thin-lens spectrometer, the modification of ring focus collection has much improved its performance in other respects. The usefulness of the spectrometer is demonstrated in the next chapter where an account is given of the investigation of the decay scheme of Sb 125.

CHAPTER III

THE GROUND STATE DECAY OF Sb 125

With a spectrometer of the characteristics described above, it is now possible to attempt an analysis of very complex decay schemes with some hope of success. A particularly complicated decay scheme is that of Sb 125 which has been investigated by other workers.[18-25] While there is general agreement on some aspects of the decay in previously published results, there is considerable disagreement on other details. In view of this fact, an analysis was performed on the radiations of Sb 125 in an attempt to resolve these differences.

I. Previous Investigation

Several research groups have studied the decay schemes of Sb 125 and Te 125 since 1949. A review article on isotopes by Strominger, Hollander, and Seaborg[26] lists the major contributors in the earlier investigation of this

decay scheme and some of these results will now be outlined.

The intensity of X-ray emission from a sample of Sb 125, known to decay by negatron emission to Te 125, led Friedlander et al[18] to look for a highly converted isomeric transition in Te 125. They observed, after chemically separating the Te 125 from the Sb 125, that the Te 125 was radioactive. From lifetime and absorption measurements on the emitted conversion electrons, they concluded that a transition of about 120 kev existed in Te 125m and that the transition was probably 2^5-pole. In a later paper by Hill et al[19], spectrographic analysis of the conversion electrons disclosed K, L and M internal conversion peaks corresponding to a 109.3 kev transition from which they obtained the intensity ratios, K/L = 1.5 and L/M = 3.5. The transition was identified as M4 with a possible 5% admixture of E5. Evidence for another transition was also observed through an internal conversion line at 30.4 kev and the half-life of the metastable state was measured to be 58 ± 4 days.

A rather thorough investigation of the decay of Te 125m was made by Bowe and Axel[20], in which they established two levels at 35.5 kev and 145.2 kev above the ground state. Branching ratios for both the 110 kev and 35 kev transitions were determined and single particle assignements of $s_{1/2}$, $d_{3/2}$ and $h_{11/2}$ were made to the ground state, 35.5 kev level and the metastable 145.2 kev level respectively. Comparison

of experimental conversion coefficients with theoretical values identified the 35 kev transition as M1 with < 1% admixture of E2.

Kern et al[21] were the first to attempt to measure the beta spectrum of Sb 125. They identified two beta groups at 288 kev and 621 kev and from photoelectron and internal conversion spectra observed gamma-rays of 110, 175, 431, 466, 609 and 646 kev. After chemical separation of the Te 125 and investigation of the internal conversion lines of the 110 kev transition, they measured its K/L ratio to be 1.2.

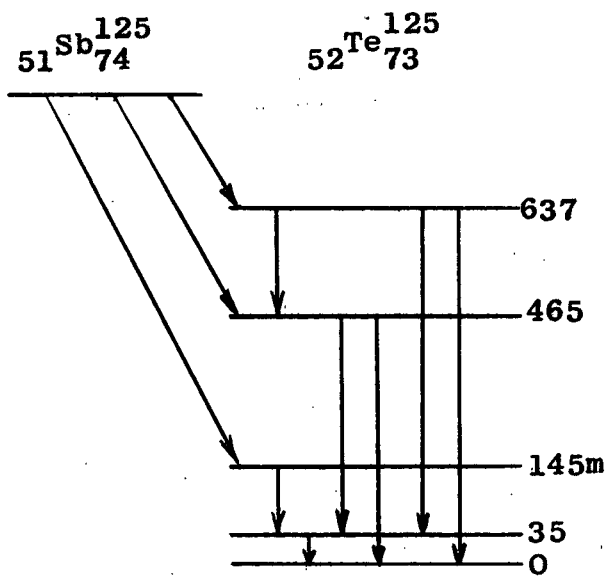

Figure 14 - Decay scheme of Siegbahn and Forsling.

Siegbahn and Försling[22] proposed the decay scheme in Fig. 14, the first suggested decay scheme that bears some resemblance to the currently accepted scheme for Sb 125. By spectroscopic analysis they observed three beta groups at 128, 299 and 616 kev which were identified as being first-forbidden, second-forbidden and third-forbidden respectively. From the internal conversion spectrum and the photoelectron spectrum, gamma-rays at 35,

110, 175, 425, 465, 601 and 637 kev were identified and the K/L+M ratio for the conversion lines of the 110 kev transition was measured to be 1.1.

Moreau[23] pointed out that the intensity of the 175 kev gamma-ray observed by Siegbahn and Forsling could not be fully accounted for by their decay scheme. He observed the same gamma-rays as they did but by measuring beta-gamma coincidences between 175 kev gamma-rays and 320 kev beta-rays he was able to establish a level 175 kev above the metastable state (145 kev) at 320 kev. Through gamma-gamma coincidences between the 425-465 kev group and gamma-rays of 175 kev he confirmed the presence of two 175 kev transitions in Te 125. Moreau's decay scheme, in Fig. 15,

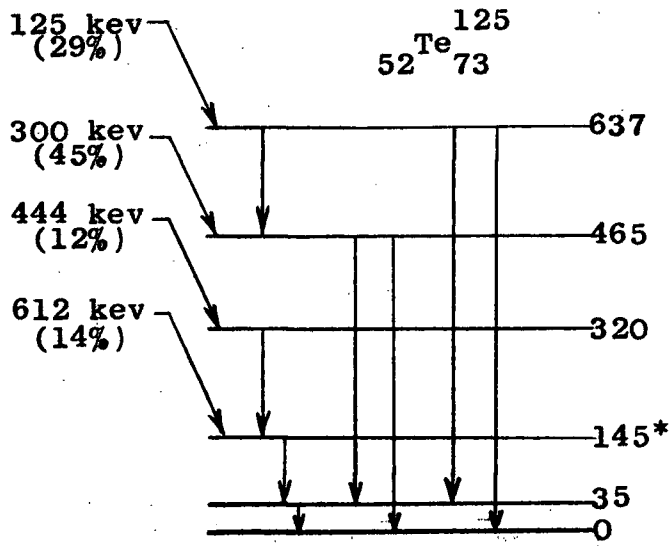

Figure 15 - Moreau's decay scheme.

included four beta groups although only the 612 kev and 300 kev groups could be easily identified in his beta spectrum. Intense internal conversion lines obscured the high energy ends of the 444 kev and 125 kev groups but the 320 kev and 637 kev levels to which these beta groups decay were easily established through the 320-175 kev beta-gamma coincidence measurement and the existence of the 601-637 kev gamma-ray group.

In 1956, Lazar[24], using scintillation counters, made a study of the gamma radiations of Te 125 by investigating gamma-gamma coincidences. He identified eleven gamma transitions, in addition to the 110 kev-35 kev cascade from the metastable state, and proposed the decay scheme shown in Fig. 16. From his measured gamma intensities and the half-life value of 2.0 ± 0.2 years for the ground state of Sb 125 he calculated the intensities of the beta groups and their log ft values. In the present investigation some reliance has been placed

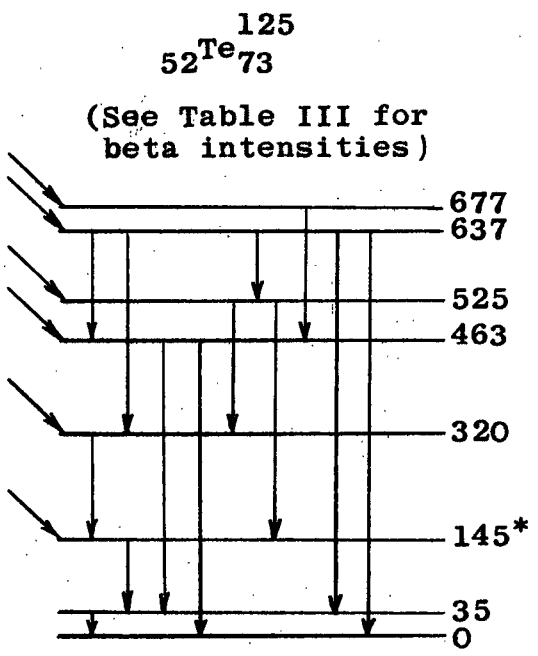

Figure 16 - Lazar's decay scheme.

on Lazar's work concerning the positioning of the 676 kev level, but this will be discussed later.

Narcisi[25] has measured the beta spectrum and photoelectron spectrum with a double-focusing spectrometer as well as gamma-gamma coincidence spectra in the study of this decay scheme. His proposed decay scheme is essentially the same as Lazar's up to the 525 kev level but instead of the 637 kev and 677 kev levels, Narcisi has established levels at 633.6, 639.7, 652 and 667.6 kev. K-shell internal conversion coefficients were calculated by Narcisi assuming that the 428 kev transition was pure E2 and had a conversion coefficient of .009 - from Sliv and Rand[27].

II. Present Investigation

While it is realized that a complete and comprehensive study of any decay scheme must necessarily involve extensive investigation of both beta and gamma radiations, the emphasis in this work is primarily on the beta radiations. This emphasis is motivated partly by the fact that the greater part of the work done on this decay scheme up to the present time has been in the study of the gamma radiations from Te 125. The beta spectrum of the ground state decay of Sb 125 has not been studied as extensively mainly because

of its complexity. For the same reason, few attempts have been made to obtain beta-gamma coincidence spectra. In the present investigation the results obtained in the measurement of the three types of spectra mentioned above appear to justify the more extensive use, once again, of the thin-lens spectrometer in nuclear spectroscopy with the incorporation of the previously described modification.

a) Methods and Apparatus

(i) Source preparation

A 1 millicurie Sb 125 source was obtained from Oak Ridge. It was in the chemical form of $SbCl_3$ and SbOCl in 6N HCl solution and was carrier free. For source-backing material, the relatively thin (240 $\mu g/cm^2$) aluminum foil used for the Cs 137 source could not be used because of the nature of the acid solution. After investigating several source-backing materials it was decided to use a thin film of collodion. Thin films were prepared by allowing a drop of a very dilute ether solution of collodion to spread over a water surface. After picking up the film from the water surface by means of a simple wire frame and then allowing it to dry, the film was mounted on an aluminum source ring. The film was then very thinly aluminized by an evaporation technique to prevent source charging. A small drop of source solution was deposited on the aluminized backing, allowed to

evaporate to dryness and then covered with another thin film of collodion to contain the source and prevent the danger of source material flaking off and contaminating the spectrometer. Source backings obtained in this way were thin enough to produce white light fringes and therefore were felt to be adequate. The source prepared in the above manner was used in the measurement of the beta spectrum and the beta-gamma coincidence spectra.

Very little source solution was used to prepare the beta source so that considerable activity was left for the preparation of a photoelectron source. Experience in this laboratory has emphasized the importance of using a thin electron absorber in a photoelectron source so that the active material may be positioned as closely as possible to the converter. This is necessary so that reasonable intensity may be obtained in the photoelectron spectrum. A complication is introduced through the fact that a thin absorber must of course be made from a material of higher Z than a thick absorber if each type is to stop electrons of a given energy. The thin absorber therefore becomes a source of photoelectrons itself since the cross-section for the photoelectric effect increases by at least Z^4. Thus the usual compromise must be made between the Z-value of the absorber and the thickness of the absorber.

The absorber used in the photoelectron source for the

present investigation was 1/64" thick copper sheet bonded to the standard type of aluminum source ring used in the spectrometer. A small indentation was made in the back of the absorber with a center punch and the entire source solution was deposited in this indentation drop by drop and evaporated to dryness, sometimes aided by heating with an infrared lamp. Collodion was then deposited in ether solution to keep the source material in the indentation. Fig. 17 illustrates the photoelectron source.

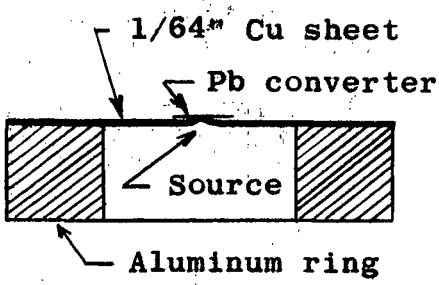

Figure 17 - Photoelectron source.

Both bismuth and lead converters were used to obtain photoelectron spectra. The bismuth converter was 4 mm in diameter and 1.86 mg/cm^2 and was prepared by evaporating bismuth onto an aluminum foil. The lead converter was 4 mm in diameter and 12 mg/cm^2 thick and was prepared by manually rolling lead sheet into a thin foil.

(ii) Apparatus - mechanical

The spectrometer has been thoroughly described in Chapter II and therefore only the particular geometric parameters chosen will be noted here. For all spectra the

following geometry was used in the spectrometer:

(a) Exit baffle diameters = 10.6 cm, 10.0 cm

(b) Entrance baffles = arctan .313, arctan .390 (ω=1.1%)

(c) Source position = 21.5 cm.

Because of the large flux of gamma rays from the Sb 125 source, particularly from the photoelectron source, three lead baffles were placed in the vacuum chamber to reduce the counting rate due to scattered photons (see Fig. 7). The baffles were experimentally positioned to avoid cutting into the electron beam. Any lead surfaces on the baffles that were exposed to the electron beam, thereby constituting a source of scattering into the beam, were covered with Apiezon Q, whose low Z-value reduces this type of scattering. One lead baffle consisted of an inner and outer portion separated by an annular slot through which the electron beam passed. This baffle was placed between the source and detector to shield the detector from direct gamma radiation from the source. Each of the other two lead baffles consisted of an outer portion only. They were placed in front of the detector and the source baffles to reduce the area of the vacuum chamber walls "seen" by the source and detector and therefore to reduce the scattering from this part of the apparatus.

For beta-gamma coincidence spectra, a modification was made to the source end of the spectrometer to allow the

positioning of a gamma detector near the source. This modification is illustrated in Fig. 18. Because of the proximity of the source and magnet, a rather high magnetic field exists in the region of the source. A 5 1/2" long lucite rod, used as a light-pipe to couple the 1 1/2" x 1" NaI(Tl) crystal to the RCA 6342 photomultiplier, removed the photomultiplier from this high field region. A lead shield with a tapered aperture collimated the photons and reduced the scattered radiation striking the crystal. A detailed account of the beta-gamma coincidence modification is given by Schneider[28].

(iii) Apparatus-electrical

The counting circuit used to measure the beta spectrum and photoelectron spectra of Sb 125 was exactly the same as the one used in the investigation of the focusing properties of the modified spectrometer This circuit is shown in Fig. 11.

The electronic circuitry used to measure the beta-gamma coincidence spectra is shown in block diagram form in Fig. 19. Basically it is a standard fast-slow triple coincidence circuit in which fast rise-time pulses from the beta and gamma detectors are fed into a coincidence unit along with other beta pulses which have first passed through a discriminator circuit. This circuit rejects many of the noise pulses, thereby improving the signal-to-noise ratio. Pulses which arrive at these three inputs in coincidence generate a gate

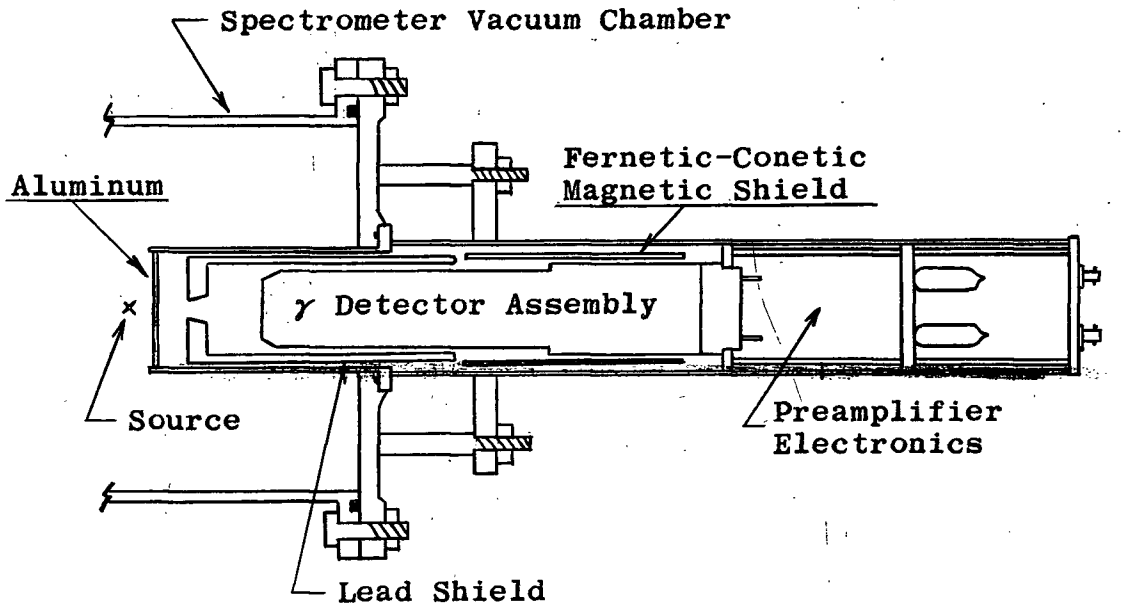

Figure 18 - Beta-gamma coincidence modification.

To follow page 61

To follow page 61

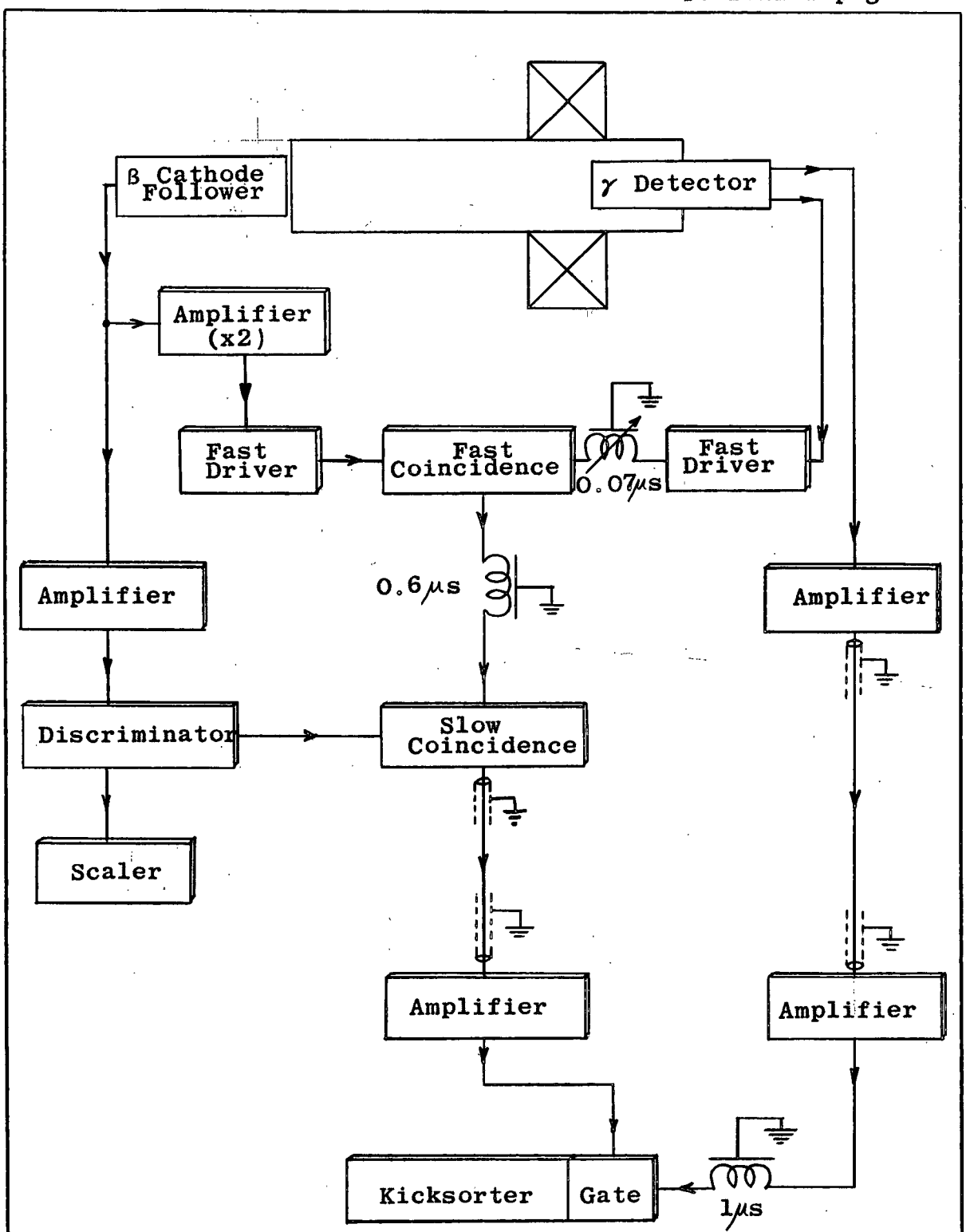

Figure 19 - Block diagram of the beta-gamma coincidence circuit.

pulse which is used to open the gate at the input of the 100-channel kicksorter. Signal pulses from the gamma detector are also fed to the kicksorter so that each time a gate pulse arrives, the gamma-ray signal pulse contributing to the triple coincidence is allowed to pass through the gate to be analyzed and stored in the appropriate channel. This fast-slow coincidence circuit is described in detail by Schneider[28].

Some minor changes in the operating voltages used by Schneider in the above circuit should be noted, however. These differences were: (a) while, for maximum gain, the screen voltage of the beta detector photomultiplier was the same as the first dynode voltage, the H.T. was increased to 1500 v; (b) because of the low energy photons in the Sb 125 spectrum, the gamma detector H.T. was increased to 1600 v; and (c) the higher H.T. on the gamma detector caused the signal generated at the eighth dynode to become nonlinear and the signal tap point was thus moved to the seventh dynode.

b) Results

The resolution obtainable with the instrument geometry chosen above varied with the particular source being studied. This was primarily due to the source size. Cs 137 was used to calibrate the beta spectrum of Sb 125 and had a line width of 1.25% on the K-shell internal conversion line of the 662 kev transition. The value used for the momentum of this

line was 3381.28 gauss-cm. In the Sb 125 beta spectrum itself, the smallest line width obtained on an internal conversion line was 1.27% on the 428 K peak, indicating that the sizes of the two sources must have been nearly the same. The line width obtained on the strongest peak in the photoelectron spectrum, on the other hand, was 3.4% but the effective source size ($\backsim$4 mm diameter) was of course considerably greater than the size ($\backsim$1 mm diameter) of the Sb 125 beta source.

(i) The beta spectrum

The beta spectrum of Sb 125, in Fig. 20, was measured by plotting the significant count rate as a function of potentiometer setting. The significant count rate was the observed count rate less the background count rate corrected for magnetic defocusing of the photomultiplier. With the aid of tables of Fermi functions, a Kurie analysis of the beta spectrum was undertaken.

It must be admitted that before the analysis was begun, the prospect of determining reliable intensities and end point energies of at least five primary beta groups by this method, did not appear to be too hopeful in view of the multiple subtractions that the process requires. The results, however, are reasonably unambiguous and surprisingly consistent with the requirements imposed by other data. The analysis revealed five distinguishable beta groups, which for purposes of discussion will be called N_1, N_2, N_3, N_4 and

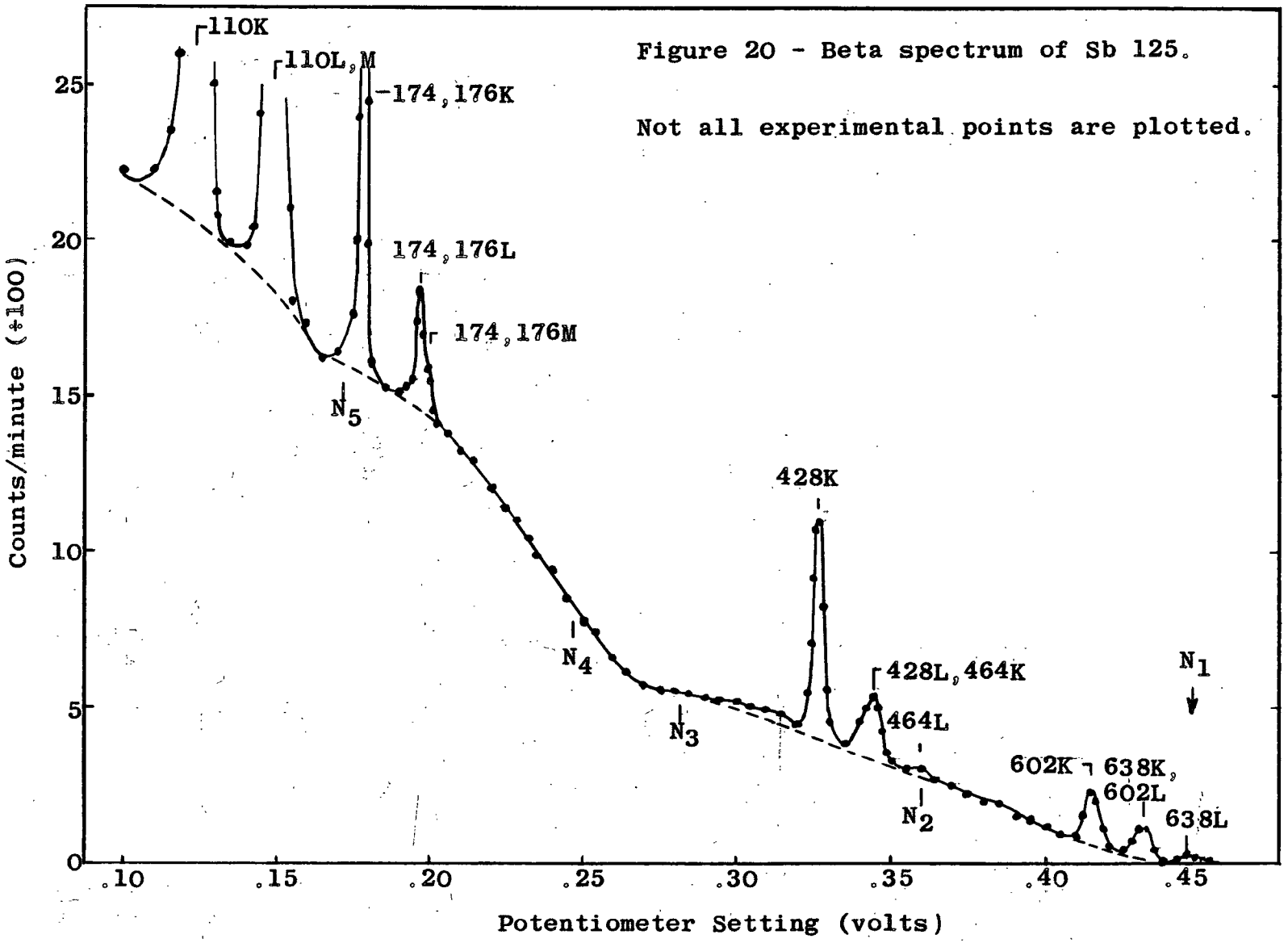

Figure 20 - Beta spectrum of Sb 125.

Not all experimental points are plotted.

To follow page 63

N_5 in decreasing order of energy.

The Kurie analysis of the N_1 group required the first-forbidden unique shape factor[5] $a_1 = W^2-1+(W_o-W)^2$ to produce a straight line, which indicated $\Delta I = 2$; "yes". A least squares calculation was made on the data resulting in an end point energy of 626.4 kev.

After subtraction of the N_1 group, the residue shows the presence of the N_2 group. Unfortunately, most of the experimental points of this group are not too reliable since the beta spectrum in this region is almost entirely covered by a group of internal conversion lines. The points used were in fact taken by making a reasonable estimate of the beta distribution under the conversion lines. Only a relatively short momentum interval in this group was free of this uncertainty. However, the end point energy of this group is known with respect to the N_1 end point energy through a connecting gamma transition. Therefore, since we were unable to trust the N_2 data sufficiently to accurately determine the shape of this group, a linear Kurie plot was drawn from the known end point, 450.4 kev, through the few points that were accurately known. This assumption of a linear Kurie plot for N_2 is not justified of course, so that the intensity of this group cannot be determined with any accuracy.

An attempt was made to determine the possible extent of this uncertainty. If it was assumed that the group was first-

forbidden unique and the appropriate shape factor correction applied to the unreliable data, then the group intensity dropped by approximately 40%. The effect of this was primarily to increase the intensity of the next group N_3 by almost the same number of counts, while groups N_4 and N_5 were essentially unaffected both in intensity and end point energy. That is, the total N_2+N_3 intensities remained effectively constant during this manipulation of the spectral shape of the N_2 group.

After subtracting the N_2 group (linear Kurie plot), the intense N_3 group displayed a linear Kurie plot with end point energy of 309.3 kev. Subtraction of the N_3 group resulted in a non-linear Kurie plot for the weak N_4 group. Applying the first-forbidden unique shape factor correction once again resulted in a Kurie plot that was linear within experimental uncertainties. Independent support for the shape factor correction to the N_4 group was the effect it had on the end point energy of the intense N_5 group which follows it in the subtraction process. When the shape factor was not applied to the N_4 group, the measured end point energy of the N_5 group and the end point energy estimated from other evidence were considerably different. Application of the shape factor reduced this discrepancy to a value more consistent with the error expected for a group as intense as N_5. The measured end point energy of the N_4 group was 247.4 kev.

After subtracting the N_4 group, the N_5 group produced a linear Kurie plot with an end point energy of 132.8 kev. Examination of the N_5 Kurie plot shows what appears to be evidence for a still lower energy beta group. Unfortunately, this is the energy region wherein one can expect absorption and scattering from the source and source backing material[5]. Therefore no further conclusions can be drawn regarding the presence of other beta groups. Other workers have presented indirect evidence for a weak beta group, N_6, with an end point energy between 90 kev and 100 kev. In this region, the N_5 Kurie plot appears to be quite linear. Hence if N_6 exists, it is quite weak compared to N_5. It has been estimated that it should be observed as an identifiable group if its intensity were greater than about 4% of the intensity of N_5. One must then admit the possibility of the existence of N_6 with an intensity less than this limit. The measured intensity of N_5 would then in fact be the intensity of N_5+N_6 combined.

The Kurie analysis plots are shown in Fig. 21.

The intensities of the beta groups were determined by plotting the momentum distribution and measuring the area under each beta group and correcting for the resolution factor (1.4%) as discussed in Appendix I. Because of the low energy detection limitations already mentioned, the measured intensity of the N_5 group was assumed to include the N_6 group. The results of this analysis are summarized in Table III.

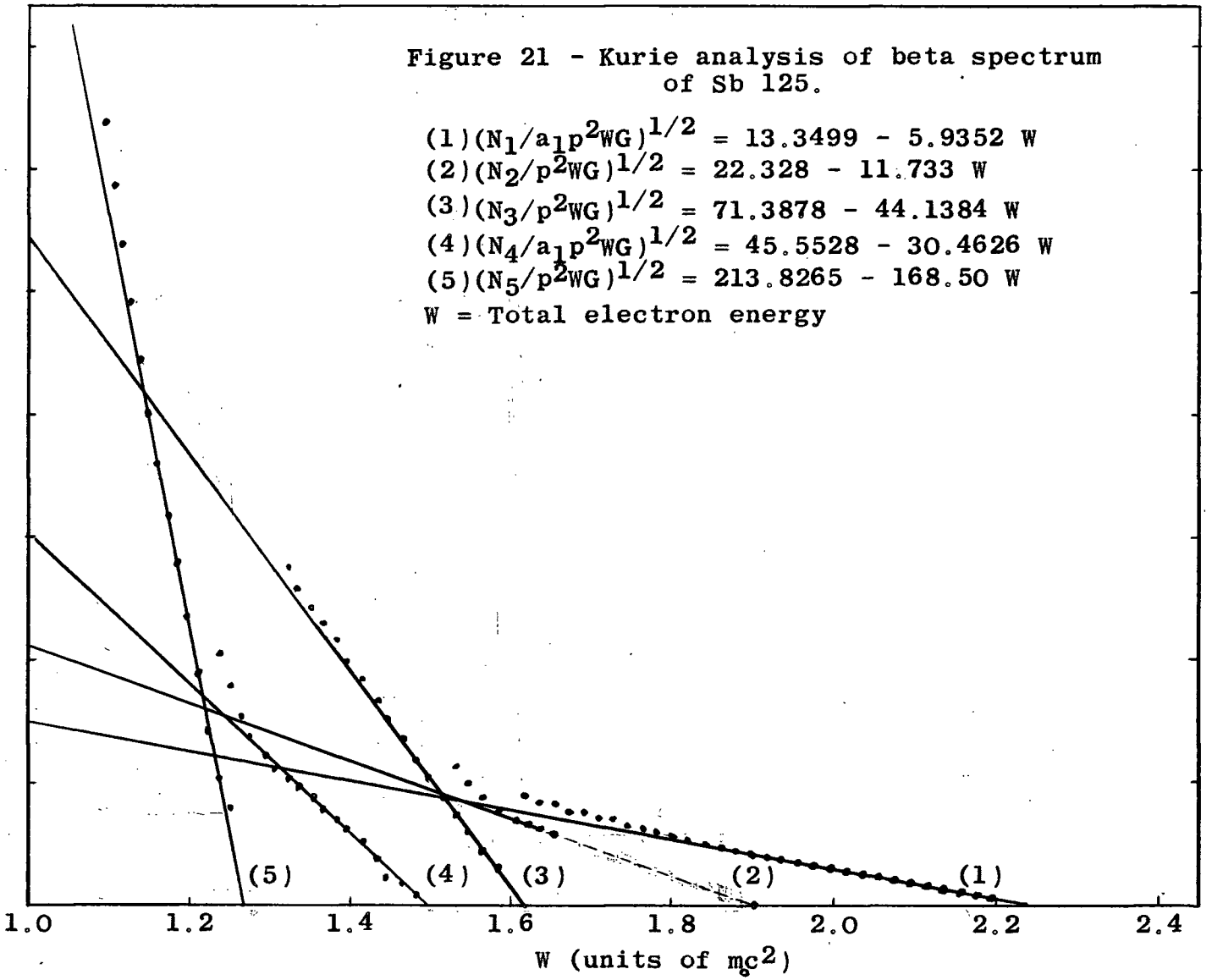

Figure 21 - Kurie analysis of beta spectrum of Sb 125.

To follow page 65

Table III. Summary of beta group intensities, end point energies (both measured and corrected) and log ft values. Bracketed entries are Lazar's results.

Group	End Point Energy Measured	Corrected	Intensity Measured	Corrected	Relative	Log ft
N_1	626.4 kev	627 kev	27,900c/m	27,900c/m	12.6% (14.0%)	9.5 (9.3)
N_2	450.4	451	20,200	~13,375	6.04 (5.5)	9.3 (9.4)
N_3	309.3	308	80,500	~87,325	39.42 (42.0)	8.0 (7.8)
N'_4	247.4	247	8,390	8,390	3.79 (1.2)	>8.6 (9.2)
N''_4		232				>8.6
N_5	132.8	134	84,400	>81,400	>36.75 (37.0)	<6.8 (6.7)
N_6	-	96		< 3,000	< 1.36 (0.17)	>7.9 (8.7)

To follow page 65

It was recognized, of course, as was stated above, that a Kurie analysis involving several subtractive processes likely imposes probable errors that increase with each subtraction, particularly when the residues involve weak groups. Thus the end point energies and intensities obtained in this manner are subject to correction from other evidence. Then, too, it is difficult to make realistic estimates of the probable errors. These errors should be smallest whenever the beta intensities are greatest but even this is subject to qualification under certain circumstances. The data for the N_1 group should be reliable since it involves no subtractions. The shape of the N_2 group is based upon an estimate of the primary beta spectrum under a group of intense internal conversion lines. This estimate affects the measured intensity of the N_2 and N_3 groups. Fortunately, analysis has shown that this effect on both the intensities and the end point energies of the lower energy beta groups is small.

The N_4 group is the weakest of all groups observed, and it is not surprising that statistical uncertainties have their greatest effect here. However, there is no doubt that this group exists; and since this region of the spectrum is free of conversion lines, estimates of its intensity should be reasonably correct. N_5 is an intense group and the data obtained from it is probably fairly reliable. The major uncertainty in N_5 of course comes from the possible inclusion

in the data of a weak N_6 group.

Table III lists two columns for the intensity and end point energy of each beta group. The first column gives the measured values determined from the Kurie analysis while the corrected column lists the results of adjustments made to these values from other data. These data are the results of coincidence experiments in which radiative and internal conversion transitions between levels fed by different beta groups establishes the end point energy differences between these groups. The transition energies are in error by not more than 0.5%. It is suprising that the adjustments of end point energies from the Kurie analysis to match the transition energy requirements are so small. Thus, one can have some confidence in the intensities resulting from the Kurie analysis. The values for the intensities of groups N_1 and N_4 are the experimentally measured values and no attempt has been made to correct them. The intensities of groups N_2, N_3, N_5 and N_6 have been established from a consistency argument, to be outlined later, but they are consistent with the experimental values of (N_2+N_3) and of (N_5+N_6).

Log ft values were calculated from the beta intensities by assuming a half-life of 2 years for the ground state of Sb 125.

(ii) <u>The internal conversion spectrum</u>

The internal conversion spectrum, shown in Fig. 22,

Figure 22 - Internal Conversion Spectrum of Te 125.

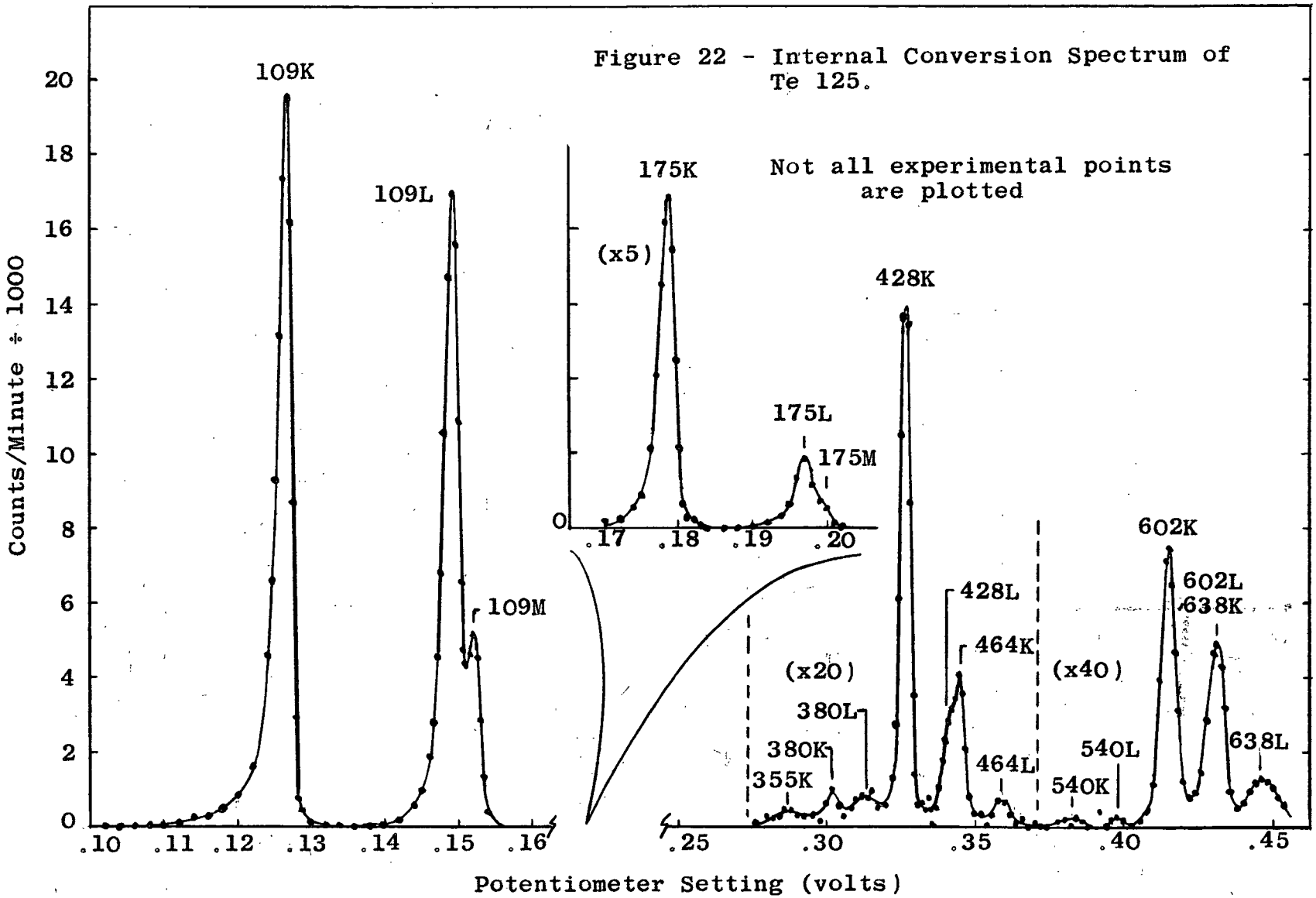

To follow page 67

was obtained by subtraction of the primary beta spectrum. As in the case of the primary spectrum, the K-shell internal conversion line of the 662 kev transition in Cs 137 was used for calibration purposes. Transitions were identified at energies of 109, 176, 355, 380, 428, 464, 540, 602 and 638 kev. Conversion line intensities are listed in Table IV and were measured by the area method discussed in Appendix I. Other methods of intensity measurement were also employed on some of the conversion lines. These methods are described in Appendix II.

(iii) The photoelectron spectrum

The photoelectron spectrum measured using the bismuth converter was of little use for measuring relative gamma-ray intensities but served to identify gamma transitions at 109, 176, 204 and 219 kev. Fig. 23 shows this spectrum and the photoelectron spectrum measured with the lead converter in which transitions at 219, 380, 428, 464, 602 and 638 kev were identified. The compton background was measured simply by removing the converter and repeating the spectrum measurements. It was necessary to "normalize" the compton background in between peaks to account for scattering effects which depend upon the presence or absence of the converter. The most important contribution of this spectrum to the present investigation was in the measurement of the 428/464 kev, 602/638 kev and 380/428 kev intensity ratios.

To follow page 68

Table IV. Internal conversion line intensities. All values are in counts/minute.

Line	Total Area	Half-Symmetry	Total Symmetry	Peak Height
109K	33,900	26,000	22,050	19,500
109L	22,000	19,600	18,470	16,400
109M	6,510	5,610	5,030	4,900
175K	2,250	1,980	1,888	1,780
175(L+M)	516			
380K				∽50
428K	692			692
428(L+M) } 464K }	330			
464(L+M)	∽45			
602K	219			
602(L+M) } 638K }	159			

Table V. Gamma-rays in coincidence with beta-rays and internal conversion electrons.

Electrons	Coincidences
N_1 group	none
N_2 group	176 kev
N_3 group	143, 176, 428, 464 kev
N_4 group	∽76, 428, 464 kev
N_5 group	602, 638 kev; possible 428, 464 kev
175K line	317 kev; possible 175 kev
428K line	possible ∽76 kev
640L line	Te 125 K x-rays

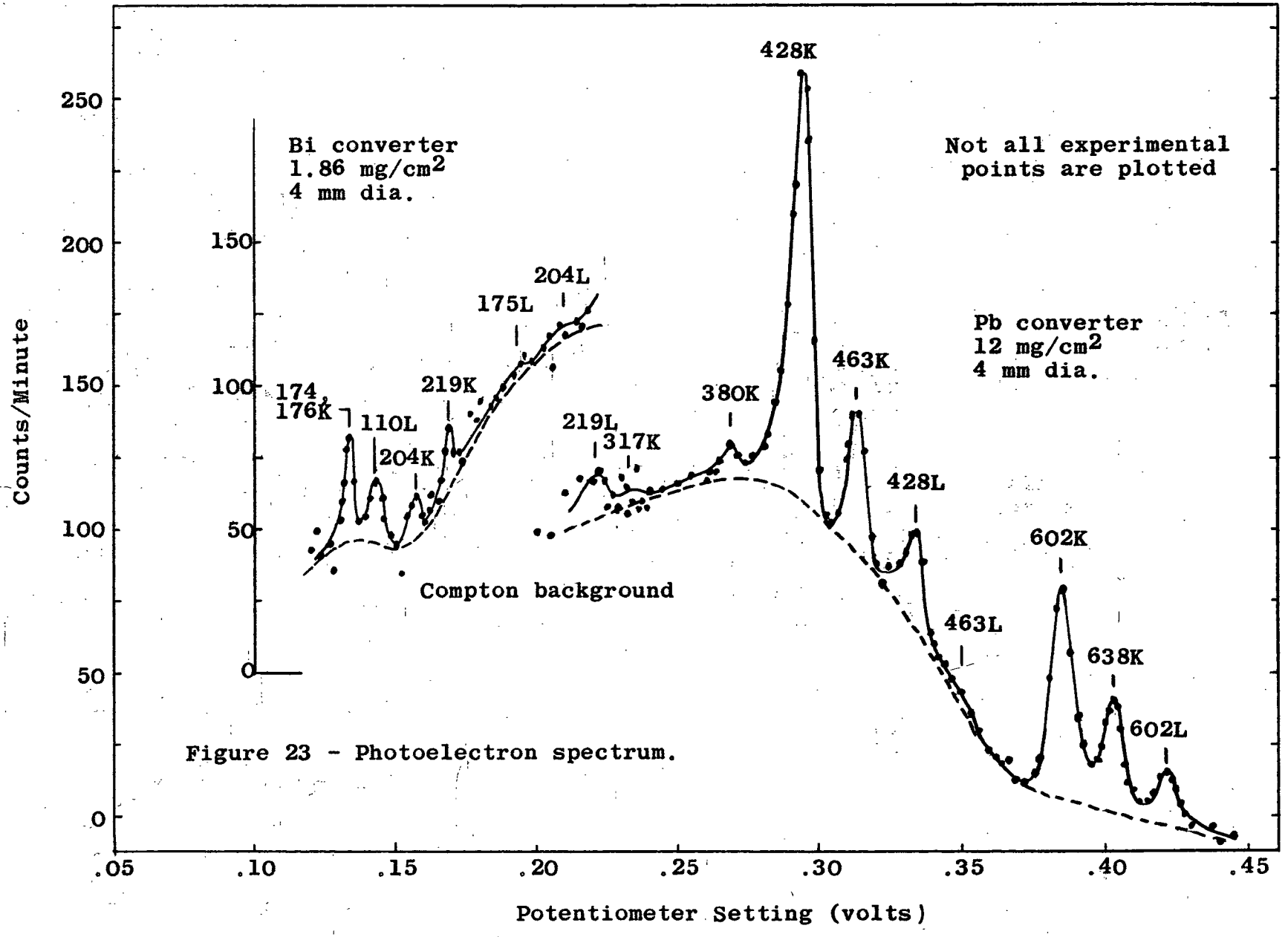

Figure 23 - Photoelectron spectrum.

To follow page 68

(iv) Beta-gamma coincidence spectra

The geometry of the gamma detector for the beta-gamma coincidence measurements was determined by the minimization of the lead x-ray produced by the gamma shield around the photomultiplier. Because of the rather intense gamma radiation from Sb 125, the x-ray could not be eliminated altogether, even with exact collimation. Thus a few preliminary singles gamma spectra were measured with different detector geometries to determine the positions of the NaI(Tl) crystal and the lead shield which gave the least x-ray interference. A typical singles gamma-ray spectrum is shown in Fig. 24.

Figures 25-29 illustrate the results of the beta-gamma coincidence measurements. Coincidence runs were taken with the magnet current set to focus electrons of energies just beyond the end point of each beta group. A series of coincidence spectra were thus measured focusing electrons from the N_1 group only, then from groups N_1 and N_2 only, then from groups N_1, N_2 and N_3 only, and so on. The coincidence spectrum measured at the potentiometer setting .370 v, which focused electrons of group N_1 only, is not shown as there were no coincidences observed, thus confirming the fact that the N_1 group feeds the metastable 145 kev level in Te 125.

Throughout the course of a coincidence run, the beta counting rate was monitored periodically. Singles gamma-ray

To follow page 69

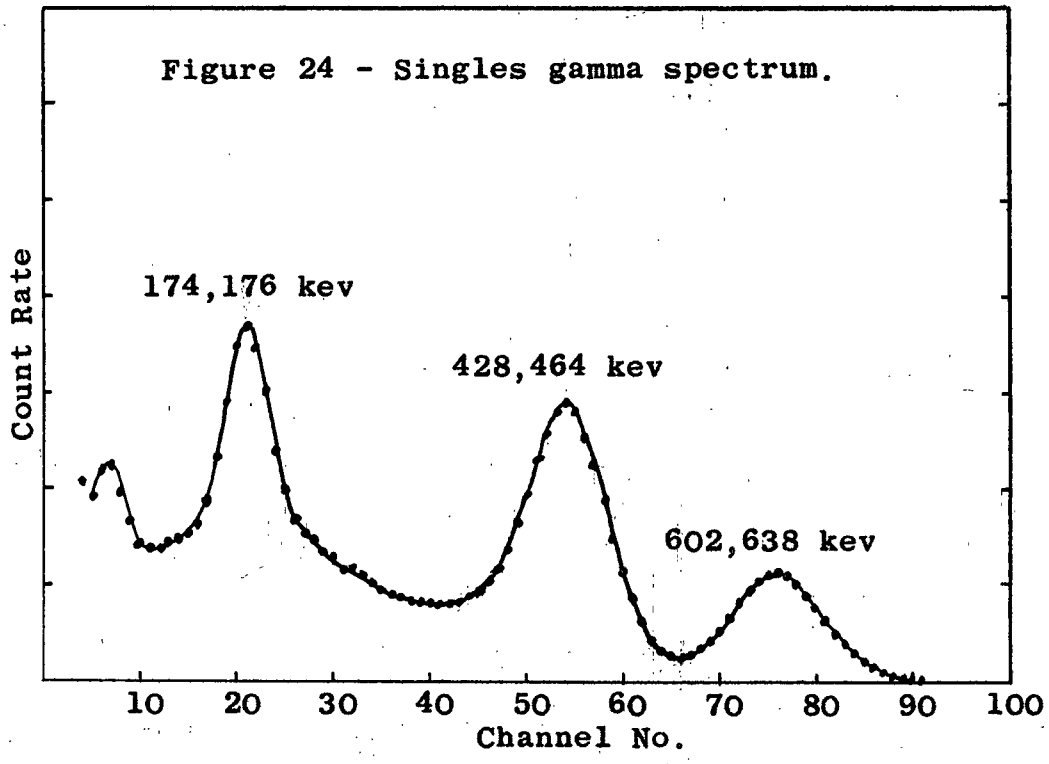

Figure 24 - Singles gamma spectrum.

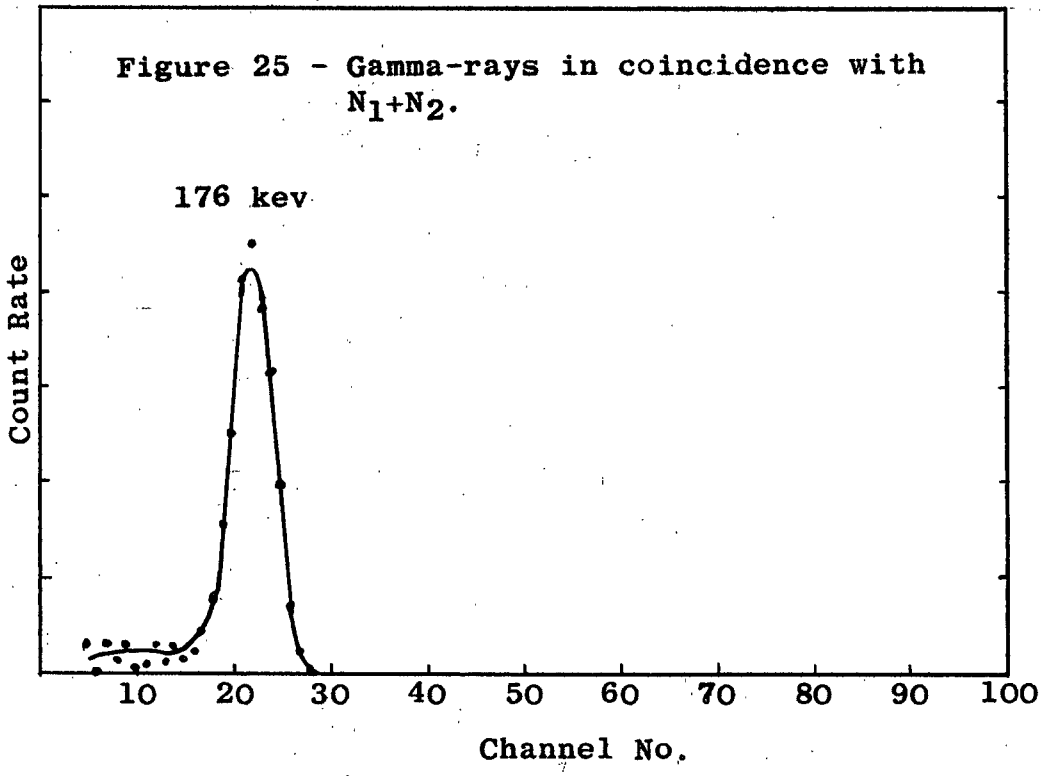

Figure 25 - Gamma-rays in coincidence with N_1+N_2.

To follow page 69

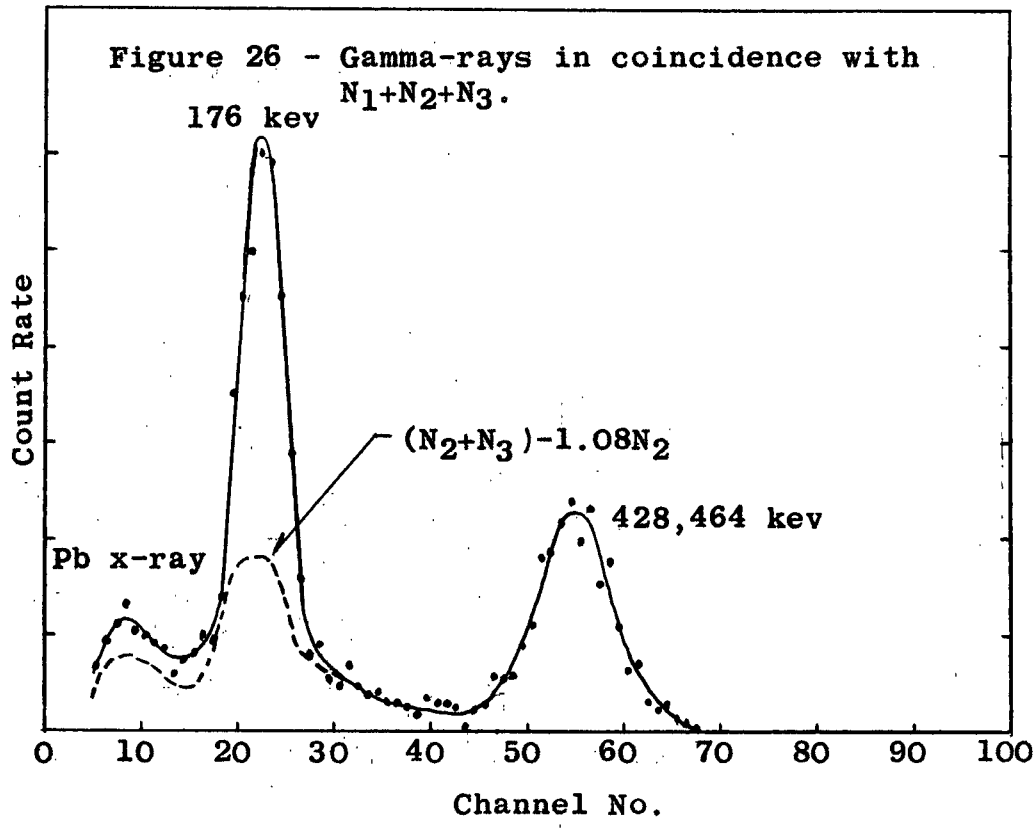

Figure 26 - Gamma-rays in coincidence with $N_1+N_2+N_3$.

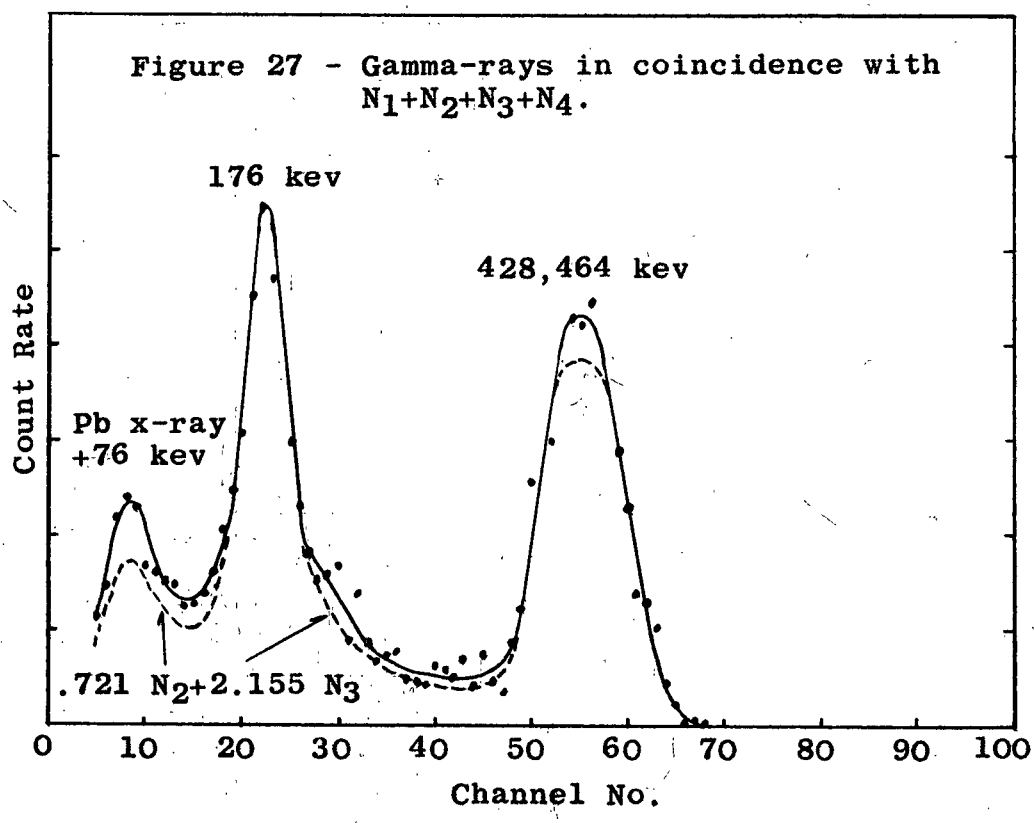

Figure 27 - Gamma-rays in coincidence with $N_1+N_2+N_3+N_4$.

To follow page 69

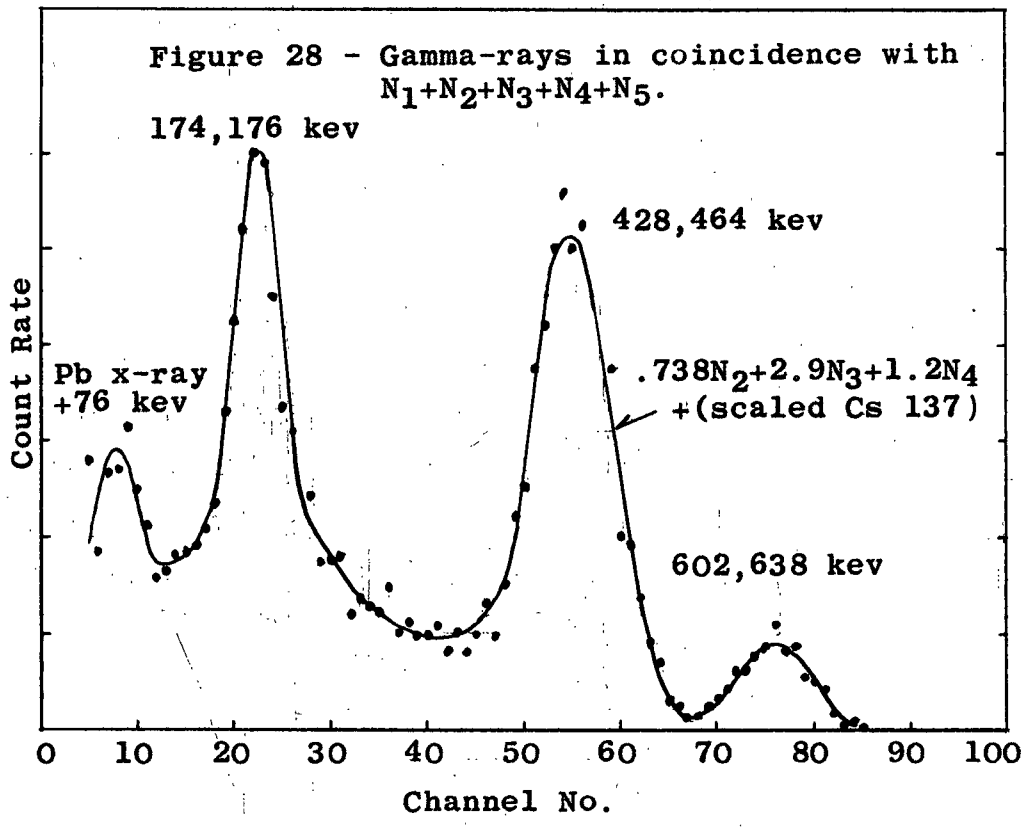

Figure 28 - Gamma-rays in coincidence with $N_1+N_2+N_3+N_4+N_5$.

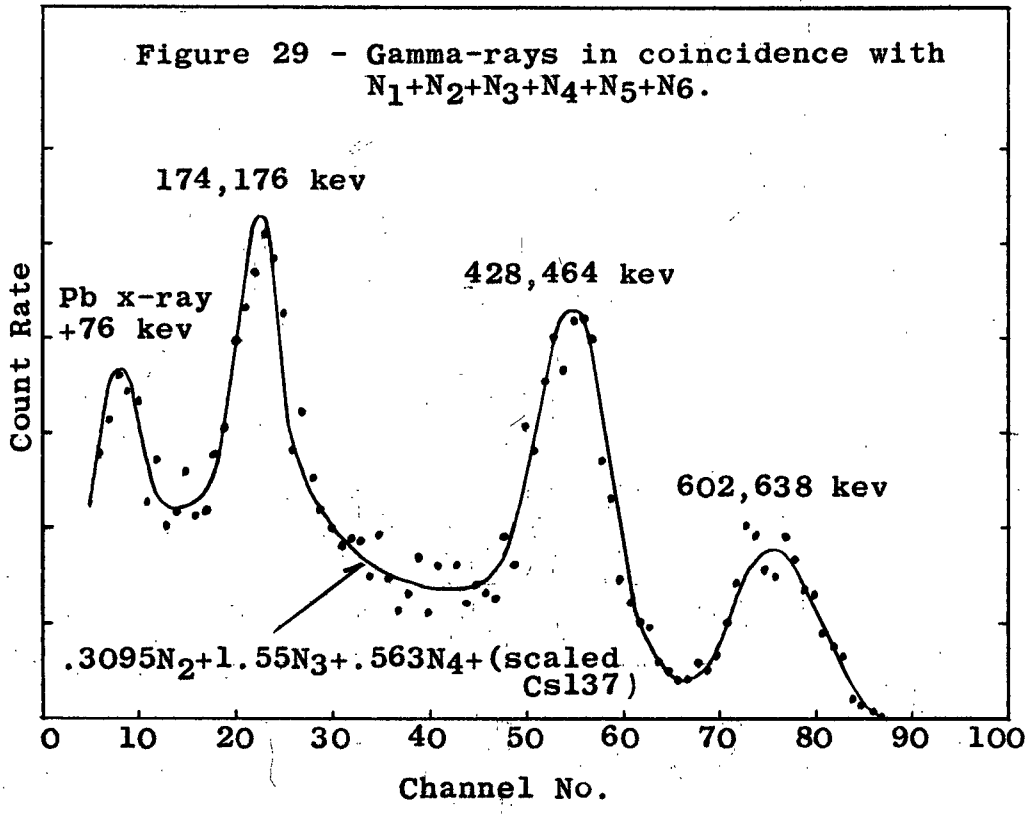

Figure 29 - Gamma-rays in coincidence with $N_1+N_2+N_3+N_4+N_5+N6$.

spectra were taken both before and after each coincidence run as a check on the system gain stability and to measure the gamma counting rate in each channel of the kicksorter. The chance coincidence rate was calculated from the formula $N_{chance} = 2n_1n_2\tau$, where n_1 and n_2 are the counting rates in the two channels and τ is the resolving time of the coincidence circuit. For the coincidence runs in the present investigation, the resolving time was measured to be 0.0975 μsec.

By successive subtractions it was possible to determine the contribution of each individual beta group to the coincidence spectrum. That is, from a knowledge of the intensity of each beta group at every potentiometer setting, as obtained from the Kurie analysis, a synthesis was made of the coincidence spectrum to be expected from any beta group at the desired potentiometer setting. For example, in Fig. 26, the solid line represents the total spectrum of gamma-rays in coincidence with electrons from groups N_1, N_2 and N_3 at the potentiometer setting .235 v and the dashed line is the residual spectrum after subtracting the expected contribution of groups N_1 and N_2. The expected contribution of groups N_1 and N_2 at the potentiometer setting .235 v is just the spectrum in Fig. 25 corrected for the relative beta-ray intensities, the change in the momentum "window" Δp and counting time differences. Thus the residual spectrum

represents the contribution of the N_3 group only, at the potentiometer setting .235 v.

The spectra shown in Figures 30 and 31 measured the coincidences between gamma-rays and the K-shell internal conversion lines of the 176 kev and 428 kev transitions.

Another set of beta-gamma coincidence runs were measured with the system gain increased so that the 176 kev gamma-ray was positioned at about channel 73 on the kicksorter. From these "expanded scale" coincidence runs, weak transitions at 76, 143, 219 and 640 kev were identified. A beta-gamma coincidence run with the L-shell internal conversion electrons of the 638 kev transition focused showed coincidences with the Te 125 K x-rays. This was interpreted as evidence for a 640 kev transition between the 676 kev level and the 36 kev level.

Table V lists the definite coincidences and possible coincidences associated with each beta group and each conversion line selected.

(v) Synthesis of the gamma spectrum

The gamma spectrum of Sb 125 was analyzed into its components by using both the singles gamma spectrum and the coincidence spectra. Cs 137 was installed in the spectrometer in the same geometry as the Sb 125 source to measure the compton contribution of the 602-638 kev group. Subtracting this contribution from the singles gamma spectrum (after

To follow page 71

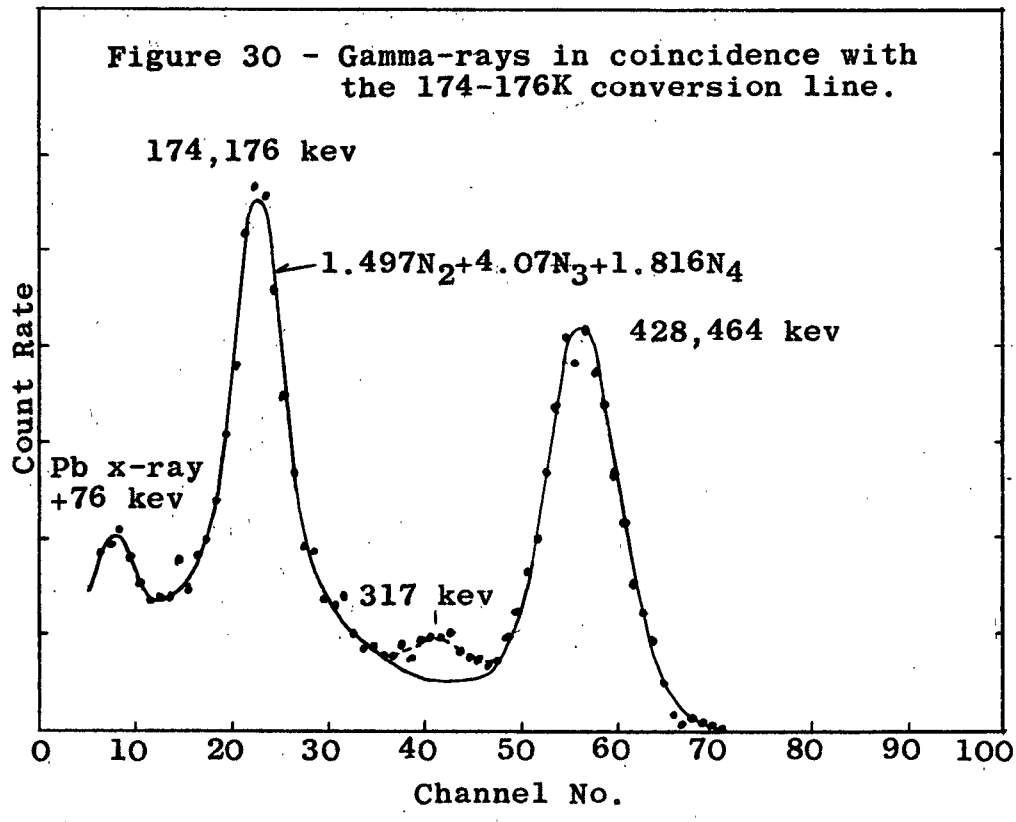

Figure 30 - Gamma-rays in coincidence with the 174-176K conversion line.

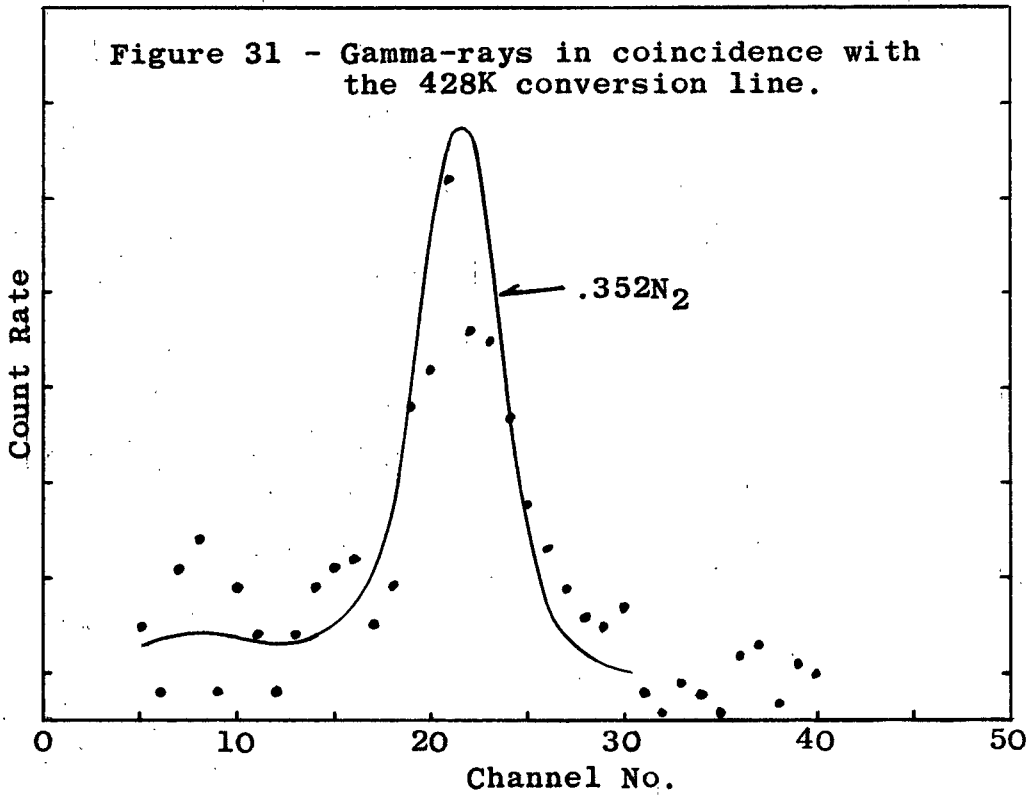

Figure 31 - Gamma-rays in coincidence with the 428K conversion line.

adjusting for energy differences) left the spectrum of the gamma-rays of energy $\leq$ 464 kev. Ideally, another source with an isolated gamma-ray of about 450 kev should have been used to determine the compton distribution of the 428-464 kev group but such a source was not available. An alternate method thus had to be employed to determine this compton contribution. The nature of the decay scheme is such that the 464 kev level decays almost entirely by the emission of the 428 kev and 464 kev gamma-rays. Thus the gamma-rays in coincidence with the N_3 group only, determined by the method of successive subtractions mentioned previously, represent the gamma spectrum of the 428-464 kev group. The 464 kev level also decays by a 143 kev-176 kev cascade which of course is in coincidence with the N_3 group as can be seen in Fig. 26. Fortunately, this cascade is weak enough so that a reasonably accurate estimate may be made of the shape of the spectrum of the 428-464 kev group alone.

After subtracting the contribution of the two high energy groups, the residual spectrum was analyzed into its various components. The last gamma-ray of major intensity in the residual spectrum was the 174-176 kev composite peak. The shape of this peak was assumed to be the same as that of the known "clean" peak obtained in the beta-gamma coincidence spectrum in Fig. 25. Subtraction of the 174-176 kev peak revealed gamma rays at 204, 219 and 380 kev. A similar

treatment of the expanded scale spectra revealed the 76 kev and 143 kev gamma-rays.

The relative intensities of the gamma-rays were calculated by measuring the area under each peak with a planimeter and correcting for photoelectric cross-section and crystal geometry efficiencies. The relative intensities of the 428 kev and 464 kev were determined by dividing the area under the composite peak into two component areas which agreed with the relative intensity results of the photoelectron spectrum in Fig. 23. A similar procedure was applied to the composite 602-638 kev peak except that the 638 kev relative intensity was adjusted to agree with the conversion coefficient for an E2 transition and the 602 kev relative intensity was taken as the difference between this value and the measured relative intensity for the composite peak. Of the weaker intensity gamma-rays, only the 380 kev gamma-ray produces a line on the photoelectron spectrum. The results of this analysis are summarized in Table VI in which comparison is made with the results of both Lazar and Narcisi. Narcisi has identified other gamma transitions for which no evidence has been found in the present investigation. These are not included in Table VI.

It should be pointed out here that analysis of a complex scintillation gamma-ray spectrum has certain fundamental difficulties which make reliable measurements of

Table VI. Relative gamma ray intensities from present investigation compared to the results of Lazar and of Narcisi.

Energy	Present Investigation	Lazar	Narcisi
∽30 kev	∽1.0	-	-
76	∽.04	-	-
143	∽.04	-	-
174-176	.209 ±10%	.196	.196
204	∽.03	.008	≤.01
219	<.01	-	-
317	<.01	.0088	.026
380	.049 ±10%	.038	.039
428	1.000 ±10%	1.000	1.000
464	.355 ±10%	.31	.325
602	.709 ± 5%	.88	.617
638	.485 ± 5%	.23	.357

relative gamma-ray intensities difficult to achieve. Any portion of the spectrum, with the exception of the highest energy portion, has at any channel, contributions not only from photoelectron peaks, but from Compton processes from gamma-rays of higher energy as well. The Compton contributions are not easy to determine precisely, and these must be known before the photoelectron residues can be estimated.

For this reason, weak gamma-ray intensities appearing in Table VI are expected to have very high probable errors and should not be taken too seriously. The most reliable intensity data will be those associated with the 638, 602, 464 and 428 kev gamma-rays. Since the 380 kev gamma-ray appears in the photoelectron spectrum as a weak peak, it can be compared with the 428 kev gamma-ray photopeak, so that its relative intensity should be reasonably correct.

The intensity of the 174-176 kev composite peak in the scintillation singles spectrum is measured after two subtractions involving somewhat uncertain Compton contributions. The relative intensity assigned to this gamma-ray consequently cannot be as accurate as the higher energy gamma-rays quoted. Finally, the x-ray-gamma peak at approximately 30 kev appears in the expanded scale spectrum at the lowest operating channels of the kicksorter. An examination of the peak shape shows a decided assymmetry, the low energy side falling off much more sharply than the high energy side. There is therefore a good chance that not all of this peak is accepted by the kicksorter, as channels 1-3 on the kicksorter are known to be inoperative. If so, then the relative intensity assigned to this peak is definitely too low.

c) <u>The Decay Scheme</u>

The decay scheme in Fig. 32 has been proposed from the

The beta information, in order, is: energy in kev, relative intensity, and log ft.

The dashed transitions are those observed by Lazar but not in the present investigation.

$^{125}_{52}Te_{73}$

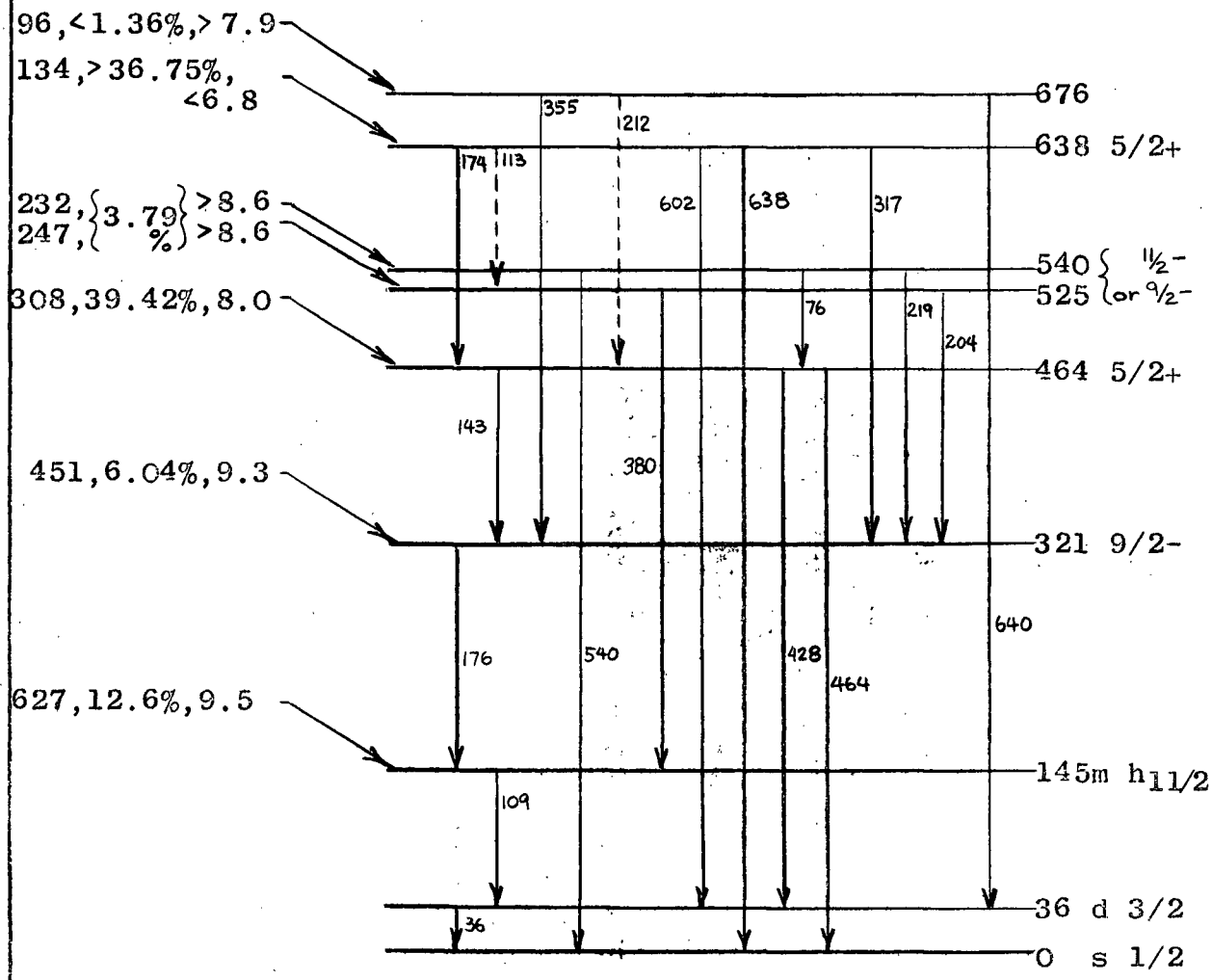

Figure 32 - Decay scheme proposed in present investigation.

present investigation with no appeal to other work except in establishing the 676 kev level as will be noted in the discussion to follow. A summary of the information obtained from the spectra is given here to facilitate the discussion of the construction of the decay scheme.

(i) Primary beta-gamma coincidence results

N_1 group: No observed coincidences.

N_2 group: In coincidence with the 176 kev gamma-ray and Te 125 x-ray.

N_3 group: In coincidence with 143, 176, 428 and 464 kev gamma-rays and Te 125 x-ray.

N_4 group: In coincidence with 76, 428 and 464 kev gamma-rays.

N_5 group: In coincidence with 602 and 638 kev gamma-rays and the Te 125 x-ray and possibly with lower energy gamma rays.

N_6 group: No observed coincidences.

(ii) Conversion electron-gamma coincidence results

174-176K: In coincidence with 317 kev gamma-ray and possibly with the 174-176 kev composite peak (weak).

428K: Possibly in coincidence with the 76 kev gamma-ray.

638L: In coincidence with the Te 125 K x-ray.

(iii) Photoelectron spectra

Transitions observed at 109, 176, 204, 219, 380, 428, 464, 602 and 638 kev.

(iv) Internal conversion spectrum

Transitions observed at 109, 176, 355, 380, 428, 464, 540, 602 and 638 kev.

Probably the most useful spectra in determining transition sequences in a decay scheme are the beta-gamma coincidence spectra. On the basis of the coincidence results, the end point energies of the primary beta groups N_1, N_2, N_3 and N_5 were adjusted to agree with the transition energies as measured in the photoelectron and internal conversion spectra. These are the corrected end point energies listed in Table III. The levels fed by these beta transitions are thus established at 145, 321, 464 and 638 kev above the ground state. The 36 kev level is established via the 428 and 602 kev transitions from the 464 kev and 638 kev levels respectively.

From the spectrum of gamma-rays in coincidence with the 174-176 K internal conversion line, a possible weak coincidence is noted between the two components of the composite 174-176 kev gamma peak. Thus the weaker 174 kev transition is established between the 638 kev and 464 kev levels. In the same coincidence spectrum, the 317 kev transition observed to be in coincidence with the composite 174-176 K internal conversion line must decay between the 638 kev and 321 kev levels rather than between the 464 kev and 145 kev levels because of intensity considerations.

The 143 kev transition is observed in the form of a composite 143-176 kev peak in the spectrum of gamma-rays in coincidence with the N_3 group. The existence of the 143 kev

transition is also evidence for the weak coincidence between the 174 kev and 176 kev transitions. While Lazar did not observe the 143 kev transition, it is not inconsistent with his spectrum of gamma-rays in coincidence with 175 kev gamma-rays in which a weak contribution exists at $\backsim$ 160 kev that could be interpreted as an unresolved 143-176 composite peak. He makes no comment on it, however, presumably because of its low intensity.

As mentioned previously, an appeal to Lazar's work is made in establishing the 676 kev level. Lazar found gamma-rays of 175 kev and 214 kev (corresponding to 174 kev and 212 kev in the present decay scheme) in coincidence with the 428-464 kev gamma group. The very definite 214 kev coincidence could only be interpreted as a transition from a level at 677 kev as in Fig. 16. In the present investigation, evidence for the existence of the 676 kev level is the 355 K internal conversion line which from energy considerations will only fit into the decay scheme between the 676 kev and 321 kev levels. Further evidence is the weak coincidence between the 638L internal conversion line and Te 125 K x-rays which is interpreted as a 640 kev transition between the 676 kev and 36 kev levels.

The observed end point energy of the N_4 group places a level of Te 125 at 525 kev. This level should be weakly populated as it is fed from the weak N_4 group. Transitions

of 204 kev and 380 kev from this level to the 321 kev and 145 kev levels respectively are easily identified. These transitions are of comparatively low intensity and this may be the reason that they are not observed in the coincidence data obtained with the N_4 group. However, N_4 definitely shows coincidences with a 76 kev transition and with the 428, 464 kev gamma group. A transition between the 525 kev and 464 kev levels of Te 125 would result in a 61 kev transition which is definitely not observed. In addition, the observed 76, 219 and 540 kev transitions still have not been accounted for.

The strong evidence that the N_4 beta group is in coincidence with the 76, 428 and 464 kev gamma rays can most easily be accounted for if the weak N_4 group is in fact a composite of two weak, unresolved beta groups of end point energies of 247 kev and 232 kev (corrected values), leading to levels in Te 125 at 525 kev and 540 kev respectively above the ground state. With this one assumption, all difficulties disappear. Not only are the coincidence data explained but the 219 kev and 540 kev transitions fall naturally into place.

If the assumption of a composite N_4 group is correct, it would be most difficult to resolve them in a Kurie analysis. Their intensities are low and their end point energies differ by only 15 kev. In addition, coincidence attempts with associated gamma-rays or internal conversion lines to resolve the N_4 components would be almost impossible because of

intensity and resolving power limitations.

The only gamma-rays observed by Lazar and not observed in this investigation are the 113 kev transition, presumably between the 638 kev and 525 kev levels, and the 212 kev transition between the 676 kev and 464 kev levels.

d) The Consistency Argument

In any decay scheme the rates of feed and decay to and from all levels must, of course, be equal. In the present investigation, the intensities of the internal conversion lines and the primary beta groups have been measured. Relative gamma-ray intensities have also been measured in the usual way. Thus a multiplying constant, K, must be found which will normalize the relative gamma-ray intensities to the beta intensities. Ideally, the calculation of the internal conversion coefficients then follows immediately and no appeal has to be made to some known conversion coefficient to normalize the conversion line intensity measurements. The value for K is determined from a consistency argument which will now be outlined.

The following equations will be understood more easily if reference is made to the decay scheme in Fig. 32 and to Tables III, IV and VI which list the relevant intensity measurements.

At each level, the total decay rate is equated to the rate of feed. For example,

676 kev level

$$N_6 = (212)+(355)+(640) \backsimeq (212)+(355) \qquad (a)$$

where (212) represents the gamma decay rate plus the internal conversion decay rate of the 212 kev transition. Here, N_6 is left to be determined from overall consistency.

638 kev level

$$\begin{aligned} N_5 &= (602)+(638)+(174)+(113)+(317) \\ &= 1.194K+400+(174)+(113)+(317) \end{aligned} \qquad (b)$$

where 1.194K = normalized decay rate of the 602 kev and 638 kev gamma-rays and 400 = total conversion electron decay rate for these two transitions. As previously mentioned, the measured intensity of the N_5 group was assumed to include the N_6 group. Thus from equations (a) and (b) we have:

$$N_5+N_6 \backsimeq 84,400 \backsimeq 1.194K+400+(174)+(113)+(317)+(212)+(355) \qquad (c)$$

N_4 levels - (both components)

$$\begin{aligned} 8390+(113) &= (76)+(219)+(204)+(540)+(380) \\ &= (76)+(219)+(204)+(540)+.049K+80 \end{aligned} \qquad (d)$$

464 kev level

$$(100,700-N_2)+(174)+(212)+(76) = (428)+(464)+(143)$$
$$= 1.355K+1100+(143) \qquad (e)$$

where it has been estimated that $N_2+N_3 \backsimeq 100,700$.

321 kev level

$$N_2+(143)+(317)+(355)+(204)+(219) = (176)$$
$$= .209K+2765-(174) \qquad (f)$$

since $(174,176) \backsimeq .209K+2765$.

145 kev level

$$27,900+(176)+(380) = (109)$$
$$(109) = .258K-(174)+30,750 \qquad (g)$$

Total decay. (Total beta feed rate = total decay to ground state)

$$221,390 = (109)+(640)+(540)+2.548K+1500$$
$$(109) = 219,870-2.548K \qquad (h)$$

A description of the detailed solution of equations (a) to (h) is tedious and in fact not necessary to the understanding of the decay scheme.

It is apparent that within the limits set by the measured data, certain parameters may be varied - e.g. the

parameter K, the intensity of $N_6 < 3000$, etc. Because of the complex nature of the decay, a poor choice of some parameters leads to predictions about the beta and gamma transitions that are inconsistent with the experimental results. It turns out, for example, that the value of K is defined within narrow limits. Thus, upper and lower limits on the K-value can be determined very simply. For example, from equation (c) one obtains:

$$K \leq 70{,}350 - \frac{(174)+(113)+(317)+(212)+(355)}{1.194}$$

while from equation (e) and (f) one obtains:

$$K \geq 61{,}910 + \frac{2(174)+(212)+(76)+(317)+(355)+(204)+(219)}{1.564}$$

Thus $61{,}910 < K < 70{,}350$. A more detailed analysis of the equations shows that the intensities of some of the weak transitions are very sensitive to the K-value. Hence the criterion for its determination was the credibility of the predicted intensities for the low intensity gamma-rays. Such a criterion has led to a K-value of $\backsim 67{,}120$. Unfortunately, little knowledge can be gained concerning the weak gamma-rays other than to impose wide limits on their intensities. However, reasonable estimates can be made on some of the adjustments to the beta intensities. These are already noted in Table III.

Some confirmation for the inner consistency of equations (a) to (h) is given by the predicted intensity of the 109 kev transition. The consistency argument predicts (109) $\backsim$ 46,250 while experimentally the value is 45,000-50,000, the uncertainty being due to the unknown source - scattering contribution to the internal conversion lines in this region of the spectrum. Appendix II gives a detailed account of the experimental measurement of the intensity of the 109 kev transition.

e) Spin and parity assignments

Work in other laboratories appears to have established with some degree of certainty the decay of the 145 kev isomeric state in Te 125. The 109 kev transition and the 36 kev transition are identified as M4 and M1 respectively. The ground state of Te 125 has been measured to be 1/2 $\hbar$ which fits well with the shell model assignment of an $s_{1/2}$ even parity state. The 36 kev level is assigned $d_{3/2^+}$ and the 145 kev level as $h_{11/2^-}$ on the assumption that for these low excitation energies, the nuclear states are genuine single particle states. Similarly, the ground state of Sb 125 is designated $g_{7/2^+}$, also in agreement with shell model predictions for a configuration representing one proton above a filled magic number shell. It is highly unlikely that the single-particle model will apply beyond these levels as

higher excitation energies will probably cause considerable configurational mixing.

The conversion coefficients for the major transitions of 175, 428, 464, 602 and 638 kev energy can now be estimated using the K-value determined from the consistency argument above. As an example, the 602 kev transition takes place with the emission of 219 K-conversion electrons/minute. The gamma-ray intensity is .709x67,120 = 47,590/min. Therefore, $\alpha_K = \frac{219}{47,590} = 4.64 \times 10^{-3}$. The theoretical values (from Rose's tables[6]) closest to this value are 4.35×10^{-3} for an E2 transition and 5.4×10^{-3} for an M1 transition. The assignment made is an E2+M1($\backsim$ 72%E2) mixture. Table VII gives the results of similar calculations for the major transitions and the multipolarity assigned to them. It has also been possible to make an estimate of the conversion coefficient for the 380 kev transition but a multipolarity cannot be uniquely assigned as theory predicts the same converstion coefficient for both E2 and M1 multipoles.

From this information, spin and parity assignments of 5/2+ have been made to the 464 kev and 638 kev levels. This is consistent with coulomb excitation experiments in which the 464 kev and 638 kev levels have been excited. Thus the 174 kev gamma-ray is an M1 transition.

The composite internal conversion line of the 174-176 kev

Table VII. Conversion coefficients and (K/L+M) ratios for the major transitions.

Transition	α_K Measured	α_K Theoretical	K/L+M Measured	K/L+M Theoretical	Multipolarity Assignment
176 kev	$\sim .14 \pm 15\%$	.18 (E2) .13 (M1)	$4.36 \pm 5\%$	3.19 (E2) 6.16 (M1)	E2+M1 ($\sim$ 60%E2)
380	$\sim 1.52 \times 10^{-2} \pm 30\%$	1.55×10^{-2} (E2orM1)	-	-	E2orM1
428	$1.03 \times 10^{-2} \pm 15\%$	1.1×10^{-2} (E2) 1.23×10^{-2} (M1)	$5.47 \pm 5\%$	5.01 (E2) 6.03 (M1)	E2+M1 ($\sim$ 55%E2)
464	$8.55 \times 10^{-3} \pm 20\%$	8.55×10^{-3} (E2) 10×10^{-3} (M1)			E2
602	$4.64 \times 10^{-3} \pm 10\%$	4.35×10^{-3} (E2) 5.4×10^{-3} (M1)			E2+M1 ($\sim$ 72%E2)
638	$3.7 \times 10^{-3} \pm 15\%$	3.7×10^{-3} (E2) 4.75×10^{-3} (M1)			E2

To follow page 85

transition is made up almost entirely of the 176 kev transition so that the conversion coefficient and the $\frac{K}{L+M}$ ratio for the composite peak are, for all practical purposes, those of the 176 kev transition alone. The E2+M1 multipole mixture assignment to the 176 kev transition thus makes the 321 kev level a 9/2- state which is not inconsistent with the information obtained from the beta spectrum.

It is worth noting that the first-forbidden unique shape of the N_1 beta group supports the $g_{7/2^+}$ and $h_{11/2^-}$ assignments to the ground state of Sb 125 and the 145 kev isomeric state of Te 125 respectively.

The log ft values for the N_4' and N_4'' beta groups are both > 8.6 indicating that they are probably first-forbidden groups ($\Delta I = 0,1,2$; "yes"). This is consistent with the shape correction factor applied to the composite N_4 group. If this is a proper correction, then either both groups are equally forbidden or one group is far more intense than the other. Therefore one might expect these levels to have odd parity and probably high spin values for reasons given in the next section. Therefore, the assignments of 9/2- or 11/2- to the N_4 levels are preferred.

Unfortunately there is not enough information to make a spin and parity assignment to the 676 kev level. The log ft value for the N_6 group (>7.9) could make the transition either allowed or first-forbidden. Then too, its low

intensity precludes the possibility of multipolarity assignments to radiative transitions originating at the 676 kev level. The low intensity of the N_6 group is probably due to the low energy available for the transition (95 kev).

f) Discussion

The apparent success of the single particle shell model in predicting the first two low-lying excited states of Te 125 is somewhat surprising. However, it is not to be expected that single particle assignments can be made to states of higher excitation energy because it is highly probable that a few core nucleons will begin to contribute to the configuration defining the spin and parity of the state.

Some justification for the single particle assignments made to the first two excited states is found in the transition probabilities predicted by the shell model for these levels. For example, for a single neutron, the transition probability, T, for an M4 transition may be roughly estimated to be (see page 391 of reference 17):

$$T = 1.5 \times 10^{-4} A^2 E_\gamma^9 S(1.8)^{-1} \text{ sec}^{-1}$$

where A = nuclear mass number, E_γ = transition energy in Mev and $S(\backsimeq 1)$ is a statistical factor. Thus for the 109 kev transition, $T \backsimeq 2.84 \times 10^{-9}$ sec^{-1}.

This may be related to the experimental half-life,

$t_{1/2}$ by:

$$T_{exp} = \frac{.693}{t_{1/2}(1+\alpha)}$$

where α is the internal conversion coefficient for the transition. For the 109 kev transition, $\alpha \simeq 293$ and $t_{1/2} \simeq 58$ days[20]. Therefore $T_{exp} \simeq .47 \times 10^{-9}$ sec^{-1}. Thus the crude estimate of the transition probability disagrees with experiment by only a factor of about six.

Te 125 has 52 protons and 73 neutrons. If we examine the predictions of the shell model in these regions, we find a cluster of close-lying levels, $S_{1/2}$, $d_{3/2}$ and $h_{11/2}$ available to the most energetic neutrons. Similarly, above the $g_{7/2}$ states which the outermost protons occupy, are two close-lying levels, $d_{5/2}$ and $h_{11/2}$. It is possible of course, that in the higher excited states these levels are violently disturbed, but if they are not, then it is not unreasonable to assume that a configuration consisting of a few nucleons of either kind, distributed amongst these available levels, would produce positive parity states of low spin (1/2, 3/2, 5/2) or negative parity states of high spin (11/2). The assignments made to the excited states of Te 125 appear to be consistent with this rather naive argument. However, if one compares the results of coulomb excitation experiments[29] in which transition probability measurements have been made for the

464 kev and 638 kev transitions with the single neutron predictions, it can be shown that these lifetimes show a greater disagreement with the predictions of the single particle shell model, the discrepancy being a factor of $\backsim 30$. For example, the transition probability for an E2 transition is given by:

$$T_\gamma(E2) = 1.23 \times 10^{-2} \, (\Delta E)^5 \, B(E2) \, \frac{2I_i+1}{2I_f+1} \quad \text{sec}^{-1}$$

where ΔE is the energy difference between the ground state and the coulomb excited state in kev, I_i and I_f are the ground state and excited state spins respectively and $B(E\lambda)$ is the reduced transition probability measured in units $e^2(10^{-24} \text{ cm}^2)^\lambda$. For the 464 kev transition, $I_i = 1/2$, $I_f = 5/2$ and $B(E2) = .44$. This gives $T_\gamma(E2) = 38.8 \times 10^9 \text{ sec}^{-1}$. The corresponding single neutron estimate of the transition probability is:

$$T = 1.6 \times 10^8 \, A^{4/3} \, E_\gamma^5 \, S \, (1.7)^{-1} \text{ sec}^{-1}$$

which leads to $T \backsimeq 1.27 \times 10^9 \text{ sec}^{-1}$. Experimental results and single particle predictions for the transition probability thus disagree by a factor of about 30. A similar discrepancy exists in the case of the 638 kev transition. At that, this discrepancy is not to be considered as very large in view of the crude nature of the single particle estimates. In other words, although undoubtedly single particle assignments are not valid here, there is apparently a faint suggestion of

shell model structure.

There are some aspects of the decay which still require verification. From the evidence obtained there seems to be little doubt of the spin and parity assignemnts made to the 145, 321, 464 and 638 kev levels. The 525 kev and 540 kev levels do not inspire so much confidence, although it is highly probable that they arise from forbidden transitions. This means negative parity and presumably high spin. The weakly populated 676 kev level is beyond our reach because of the low intensity of the radiations to and from it.

It would be useful to attempt a more accurate determination of the intensities of some of the weaker transitions to see if multipolarities could be assigned which were consistent with the quantum description of the Te 125 levels which they connect. This will require a stronger source than was available for this experiment.

APPENDIX I

INTENSITY MEASUREMENT OF CONVERSION LINES AND PRIMARY BETA GROUPS

The ring focus collection modification to the thin-lens spectrometer has given it a rather unique property among beta-ray spectrometers. That is, when the previously discussed condition of a "match" is realized, an internal conversion line displays a symmetric peak shape provided that it is of sufficiently high energy to be out of the region of source-scattering. This symmetry property is useful, in fact, for indicating the region where source-scattering begins to introduce peak distortion into the spectrum.

As previously noted, all electrons passing through the exit slot are counted by the detector. Thus, at a match, the peak height of a conversion line on an N(p) versus p plot is interpreted as the intensity of the line; and one does not need to appeal to the usual method of measuring the area under the line on an $\frac{N(p)}{p}$ versus p plot. Such an intensity measurement, of course, cannot be made on a continuous primary beta spectrum or on conversion lines which have

suffered from source-scattering. It is useful to determine the relationship between the two types of intensity measurements on a conversion line (i.e. from peak heights on an N(p) versus p plot and from areas on an $\frac{N(p)}{p}$ versus p plot), since this then gives a simple method of measuring primary beta spectrum intensities.

Let N_o be the peak height of a "clean" internal conversion line having shape N(p). Since it is a property of magnetic spectrometers that $\Delta p = kp$, where k is a constant and Δp is the line width at half height, then,

$$N(p) = n(p)\ \Delta p$$
$$= n(p)\ kp$$

where n(p) is an equivalent momentum density distribution resulting from instrumental behaviour. Thus k must be adjusted so that

$$\int n(p)\ dp = N_o = \frac{1}{k} \int \frac{N(p)}{p}\ dp$$

Reference to Fig. 33 shows the graphical representation of these equations. Curve A is simply the plot of $\frac{N(p)}{p}$ versus p while the rectangle B is the same height as curve A and has an area equal to the area under curve A. That is,

$$\frac{N_o}{p}\ (\Delta p)' = \int \frac{N(p)}{p}\ dp = kN_o$$

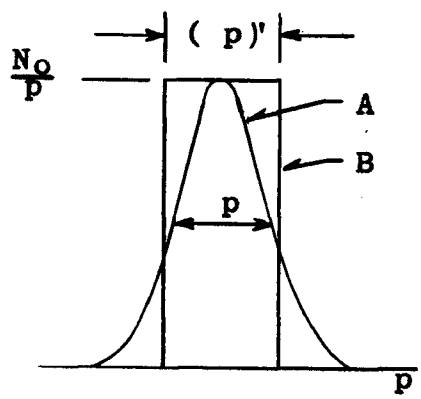

Figure 33 - Method of measuring conversion line intensity.

Therefore, $k = \frac{(\Delta p)'}{p}$. If curve A were triangular in shape, then $(\Delta p)' = \Delta p$, and k would be identical with the line width $k = \frac{\Delta p}{p}$. Since conversion lines from this spectrometer are gaussian-like in shape, then $(\Delta p)' > \Delta p$ and k is always greater than the line width. For example, on a Cs 137 internal conversion line having a line width of 1.25%, k is 1.37%. In the present investigation, the 428 K conversion line in the Sb 125 beta spectrum displayed a line width of 1.28% while the required k to make area and peak height methods of intensity measurements agree was 1.40%. This was the resolution factor used to calculate the beta intensities in Chapter II according to the equation $N_\beta = \frac{1}{k} \int \frac{N(p)}{p} dp$.

APPENDIX II

ITERATIVE METHOD OF CONVERSION LINE SEPARATION

During the analysis of the internal conversion spectrum of Te 125, it was desired to separate the unresolved 109L and 109M conversion lines. This is most often done by trial and error methods but it can also be accomplished by another method which will now be outlined.

Consider, for example, the composite peak in Fig. 34. Let the composite peak, S(x), consist of two component peaks $N_1(x)$ and $N_2(x)$ located at x_1 and x_2 respectively. Let the "position ratio" $\frac{x_2}{x_1} = s$ and the peak height ratio $\frac{N_{O1}}{N_{O2}} = r$. By the constant resolution property of magnetic spectrometers, $N_2(x)$ may be written in terms of $N_1(x)$ as:

$$N_2(x) = \frac{1}{r} N_1 \left(\frac{x}{s}\right)$$

Since S(x) is the sum of $N_1(x)$ and $N_2(x)$, then:

$$S(x) = N_1(x) + \frac{1}{r} N_1 \left(\frac{x}{s}\right)$$

and therefore,

$$N_1(x) = S(x) - \frac{1}{r} N_1\left(\frac{x}{s}\right)$$

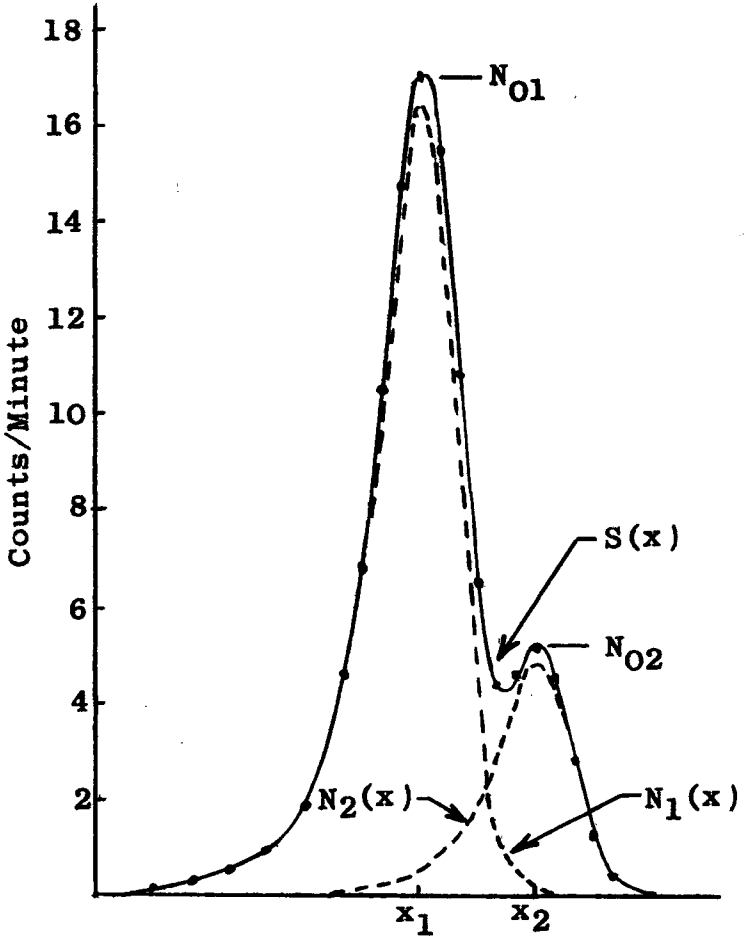

Figure 34 - Separation of 109L and 109M internal conversion lines.

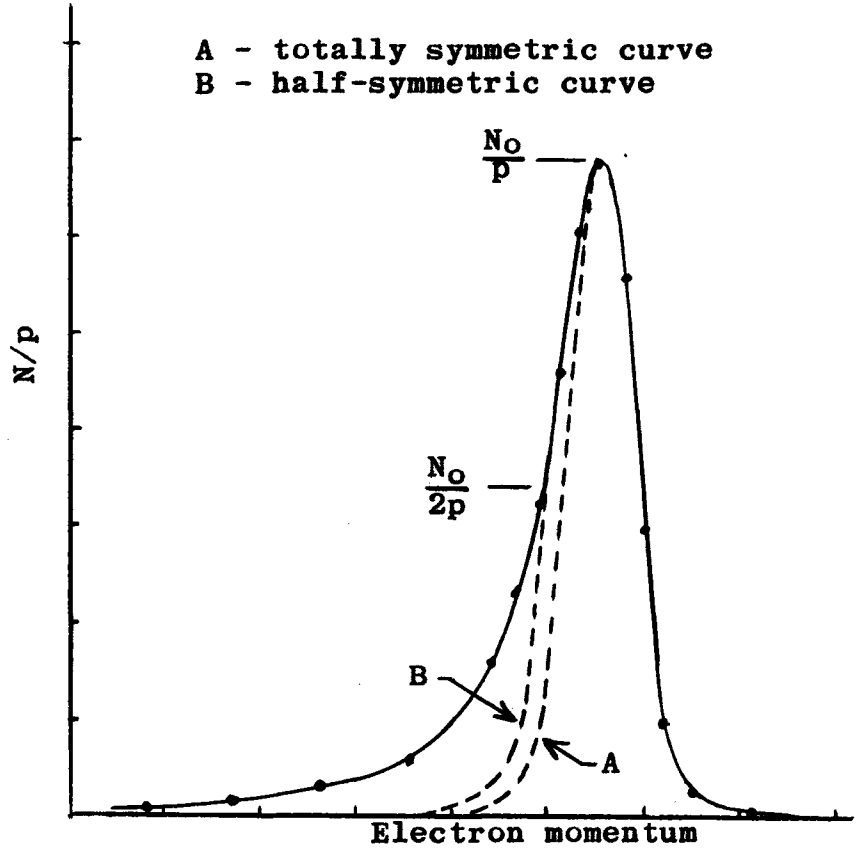

Figure 35 - Intensity measurements of the 109K internal conversion line.

To follow page 94

Repeated substitution of this equation into itself leads to:

$$N_1(x) = S(x) - \frac{1}{r} S\left(\frac{x}{s}\right) + \frac{1}{r^2} S\left(\frac{x}{s^2}\right) - \frac{1}{r^3} S\left(\frac{x}{s^3}\right) + \ldots$$

Thus $N_1(x)$ may be easily determined when r and s are known. In practice the position ratio, s, can usually be estimated with reasonable accuracy by simple inspection. The peak height ratio, r, must, however, be arrived at through an iterative process. This requires knowledge of the peak shape $N_1(x)$ which may be gained from an adjacent completely resolved conversion line in the spectrum or by making reasonable assumptions from the composite peak itself.

In the present investigation, the contributions of the 109L line at the 109M position and vice versa were determined by assuming their shapes to be the same as the 109K peak. In first approximation, the peak heights of the 109L and 109M peaks were taken to be 17,000 c/m and 5200 c/m respectively. These values were taken from the position of the maxima on the composite peak S(x) and are therefore too high. Successive approximations to the peak heights were:

109L: 17,000 ; 16,467 ; 16,472 ; 16,473

109M: 5,200 ; 4,900 ; 4,931 ; 4,933

Thus the peak height ratio was 16,473/4,933 = 3.34 = r.

Using this value for r and the measured value for s, the component peak shapes were easily determined from the equation derived above.

Because the 109K, L and M conversion lines lie in the source-scattering region, intensity measurements by any method are subject to some uncertainty. The low energy side of each conversion line has a long tail containing extra counts. There is no way to accurately measure the scattering contribution to the line intensities, although estimates can be made based on reasonable but rather artificial postulates. For example, the intensity of the 109K conversion line in Fig. 35 has been measured by four different methods. The peak height on an N versus p plot is 19,500 counts/minute while the area method, discussed in Appendix I, gives 33,900 c/m. Obviously the first value is too low because of source absorption and the second value is too high because of the excess counts under the peak. Two other completely arbitrary methods have been used to estimate the peak intensity, both measurements being derived from peak shape constructions. One method is to completely symmetrize the peak with respect to the trailing edge. This is curve A in Fig. 35. The other method symmetrizes the peak from the half-height position downwards. This is curve B. The totally symmetric curve leads to an intensity of 22,050 c/m while the half-symmetric curve leads to an intensity of 26,000 c/m. The 109L and 109M conversion lines were treated similarly and the resulting intensities are

listed in Table VIII along with the K/L and L/M ratios. The

Table VIII. Intensity measurements of the internal conversion lines of the 109 kev transition by four methods described in the text.

	Peak Height	Total Symmetry	Half-Symmetry	Total Area
109K	19,500 c/m	22,050 c/m	26,000 c/m	33,900 c/m
109L	16,400	18,470	19,600	22,000
109M	4,900	5,030	5,610	6,510
Totals	40,800	45,550	51,210	62,410
L/M ratio	3.35	3.67	3.49	3.38
K/L ratio	1.190	1.194	1.327	1.540

totals lead to the intensity estimate for the 109 kev transition of 45,000-50,000 c/m as noted in the section dealing with the consistency argument in Chapter III.

From Table VIII it is easily seen that L/M ratio is little affected by the type of intensity measurement employed. This is undoubtedly due to the proximity of the 109L and 109M lines in the spectrum. The K/L ratio, on the other hand, depends upon the type of measurement employed. The ratio derived from the total area method is undoubtedly too high for reasons already explained. The same may possibly be said of the half-symmetric method. The totally symmetric method, when applied to the K, L and M lines shows a continuous

degradation in line width as might be expected from source absorption alone. This degradation tends to reduce the discrepancy between the area method of intensity measurement and the peak height method on an undistorted line. Thus the totally symmetric method may be a reasonably close measure of the actual intensities. If so, this leads to a K/L ratio of $\backsim$ 1.2 and an L/M ratio of $\backsim$ 3.5 in fair agreement with published results[20,22].

BIBLIOGRAPHY

1. E. Fermi, Zeit. f. Phys. 88, 161 (1934).
2. E. Feenberg and G. Trigg, R.M.P. 22, 399 (1950).
3. S. A. Moszkowski, Phys. Rev. 82, 35 (1951).
4. "Beta- and Gamma-Ray Spectroscopy" - Appendix II, Edited by K. Siegbahn.
5. C. S. Wu, R.M.P. 22, 386 (1950).
6. M. E. Rose, "Internal Conversion Coefficients" - North-Holland Publishing Co.
7. L. E. Biedenharn and M. E. Rose, R.M.P. 25, 746 (1953).
8. T. R. Gerholm, Handbuch der Physik - Volume XXXIII.
9. Kofoed-Hansen, Lindhard and Nielsen, Kgl. Danske Ved. Selsk. Matfys. Medd. 25, No. 16 (1950).
10. Hornyak, Lauritsen and Rasmussen, Phys. Rev. 76, 731 (1949).
11. Keller, Koenigsberg and Paskin, Rev. Sci. Instr. 21, 713 (1950).
12. Pratt, Boley and Nichols, Rev. Sci. Instr. 22, 92 (1951).
13. Jensen, Laslett and Pratt, Phys. Rev. 75, 458 (1949).
14. Deutsch, Elliott and Evans, Rev. Sci. Instr. 15, 178 (1944).
15. D. C. Milley, M.A.Sc. Thesis, UBC (1955).
16. Fleishman, Einbinder and Wu, Rev. Sci. Instr. 30, 1130 (1959).
17. "Beta- and Gamma-Ray Spectroscopy", edited by K. Siegbahn.
18. Friedlander, Goldhaber and Scharff-Goldhaber, Phys. Rev. 74, 981 (1948).

19. Hill, Scharff-Goldhaber and Friedlander, Phys. Rev. 75, 324 (1949).

20. J. C. Bowe and P. Axel, Phys. Rev. 85, 858 (1952).

21. Kern, Mitchell and Zaffarano, Phys. Rev. 76, 94 (1949).

22. K. Siegbahn and W. Försling, Ark. f. Phys. 1, 505 (1949/50).

23. J. Moreau, Ark. f. Phys. 7, 391 (1954).

24. N. H. Lazar, Phys. Rev. 102, 1058 (1956).

25. R. S. Narcisi, AECU - 4336 (1958).

26. Strominger, Hollander and Seaborg, R.M.P. 30, 585 (1958).

27. Sliv and Rand, "K-shell Internal Conversion Coefficients", AEC-TR-2888 (1956).

28. H. R. Schneider, Ph.D. Thesis, UBC (1961).

29. Alder, Bohr, Huus, Mottelson and Winther, R.M.P. 28, 432 (1956).